



HAL
open science

Real time visualisation of conjugation reveals the molecular strategy evolved by the conjugative F plasmid to ensure the sequential production of plasmid factors during establishment in the new host cell

Agathe Couturier, Chloé Virolle, Kelly Goldlust, Annick Berne-Dedieu, Audrey Reuter, Sophie Nolivos, Yoshiharu Yamaichi, Sarah Bigot, Christian Lesterlin

► **To cite this version:**

Agathe Couturier, Chloé Virolle, Kelly Goldlust, Annick Berne-Dedieu, Audrey Reuter, et al.. Real time visualisation of conjugation reveals the molecular strategy evolved by the conjugative F plasmid to ensure the sequential production of plasmid factors during establishment in the new host cell. 2022. hal-03821610v1

HAL Id: hal-03821610

<https://hal.science/hal-03821610v1>

Preprint submitted on 19 Oct 2022 (v1), last revised 2 Jun 2023 (v2)

HAL is a multi-disciplinary open access archive for the deposit and dissemination of scientific research documents, whether they are published or not. The documents may come from teaching and research institutions in France or abroad, or from public or private research centers.

L'archive ouverte pluridisciplinaire **HAL**, est destinée au dépôt et à la diffusion de documents scientifiques de niveau recherche, publiés ou non, émanant des établissements d'enseignement et de recherche français ou étrangers, des laboratoires publics ou privés.

1 **Real time visualisation of conjugation reveals the molecular strategy evolved by the**
2 **conjugative F plasmid to ensure the sequential production of plasmid factors during**
3 **establishment in the new host cell**

4

5 Agathe Couturier^a, Chloé Virolle^a, Kelly Goldlust^a, Annick Berne-Dedieu^a, Audrey Reuter^a, Sophie
6 Nolivos^a, Yoshiharu Yamaichi^b, Sarah Bigot^{a*} and Christian Lesterlin^{a*}

7

8 ^aMolecular Microbiology and Structural Biochemistry (MMSB), Université Lyon 1, CNRS, Inserm,
9 UMR5086, 69007, Lyon, France

10 ^bInstitute for Integrative Biology of the Cell (I2BC), Université Paris-Saclay, CEA, CNRS, 91198
11 Gif-sur-Yvette, France.

12

13 * Corresponding author: Christian.lesterlin@ibcp.fr, Sarah.Bigot@ibcp.fr

14

15 **Abstract**

16 DNA conjugation is a contact-dependent horizontal gene transfer mechanism responsible for
17 disseminating drug resistance among bacterial species. Conjugation remains poorly characterised at
18 the cellular scale, particularly regarding the reactions occurring after the plasmid enters the new host
19 cell. Here, we use live-cell microscopy to visualise the intracellular dynamics of conjugation in real
20 time. We reveal that the transfer of the plasmid in single-stranded DNA (ssDNA) form followed by
21 its conversion into double-stranded DNA (dsDNA) are fast and efficient processes that occur with
22 specific timing and subcellular localisation. Notably, the ss-to-dsDNA conversion is the critical step
23 that governs the timing of plasmid-encoded protein production. The leading region that first enters
24 the recipient cell carries single-stranded promoters that allow the early and transient synthesis of
25 leading proteins immediately upon entry of the ssDNA plasmid. The subsequent ss-to-dsDNA
26 conversion turns off leading gene expression and licences the expression of the other plasmid genes
27 under the control of conventional double-stranded promoters. This elegant molecular strategy evolved
28 by the conjugative plasmid allows for the timely production of factors sequentially involved in
29 establishing, maintaining and disseminating the plasmid.

30

31

32 **Keywords**

33 Horizontal gene transfer, bacterial DNA conjugation, drug-resistance dissemination, live-cell
34 microscopy, plasmid transfer

35 **Introduction**

36 Bacterial DNA conjugation is a widespread horizontal gene transfer mechanism in which genetic
37 information is transmitted from a donor to a recipient cell by direct contact (Cruz et al., 2010;
38 Grohmann et al., 2003; Lederberg and Tatum, 1946; Virolle et al., 2020). Conjugation is responsible
39 for the intra- and inter-species dissemination of various metabolic properties and accounts for 80%
40 of acquired resistances in bacteria (Barlow, 2009). The F plasmid was the first conjugative element
41 discovered (Lederberg and Tatum, 1946; Tatum and Lederberg, 1947) and is now documented as the
42 paradigmatic representative of a large group of conjugative plasmids widespread in *Escherichia coli*
43 and other Enterobacteriaceae species, in which they are associated with the dissemination of colicins,
44 virulence factors, and antibiotic resistance (Fernandez-Lopez et al., 2016; Johnson et al., 2016; Lanza
45 et al., 2014). Due to their fundamental and clinical importance, F-like plasmids have been the focus
46 of extensive studies that provided a detailed understanding of the molecular reactions and factors
47 involved in their transfer by conjugation (*see* (Cruz et al., 2010; Virolle et al., 2020).

48 Within the donor cell, the relaxosome components, including the integration host factor IHF,
49 plasmid-encoded accessory proteins TraY, TraM and the multifunctional relaxase TraI (VirD2), are
50 recruited to the origin of transfer (*oriT*) of the F plasmid (Howard et al., 1995; Nelson et al., 1993;
51 Schildbach et al., 1998). The relaxosome complex is then recruited to the Type IV secretion system
52 (T4SS) by the coupling protein TraD (VirD4), resulting in the formation of the pre-initiation complex
53 (Beranek et al., 2004; Gomis-Rüth et al., 2004; Lang and Zechner, 2012; Llosa et al., 2003; Schröder
54 and Lanka, 2005). It is proposed that the establishment of the mating pair induces a still
55 uncharacterised signal that activates the pre-initiation complex. Then, TraI introduces a site- and
56 strand-specific DNA cut (nick) into the plasmid's *oriT* and remains covalently bound to the 5'
57 phosphate end. TraI also serves as a helicase that extrudes the ssDNA plasmid to be transferred, called
58 the T-strand (Clewell and Helinski, 1970; Dostál and Schildbach, 2010; Everett and Willetts, 1980;
59 Lanka and Wilkins, 1995; Matson and Morton, 1991; Matson and Ragonese, 2005; Reygers et al.,
60 1991; Traxler and Minkley, 1988; Willetts and Skurray, 1980). It was initially suggested and later

61 confirmed that two relaxases are required to carry out these functions (Dostál et al., 2011; Ilangovan
62 et al., 2017). At this stage, the 3'OH of the T-strand serves to initiate the rolling-circle replication
63 (RCR) that converts the intact circular ssDNA plasmid into dsDNA in the donor cell (Cruz et al.,
64 2010; Llosa et al., 2002; Wawrzyniak et al., 2017), while the 5'phosphate bound to TraI is transferred
65 into the recipient cell through the T4SS machinery. If the molecular structure of the T4SS has been
66 well characterised (Christie et al., 2014; Fronzes et al., 2009; Grohmann et al., 2018; Macé et al.,
67 2022), the way the T-strand-TraI nucleoprotein complex is translocated through the membrane of the
68 donor and recipient cells' membranes remain unclear.

69 The first transferred segment is the ~13.5 knt leading region, carrying genes which encode the
70 Ssb^F protein homolog to the chromosomally encoded essential single-strand-binding protein Ssb, the
71 PsiB protein (Plasmid SOS Inhibition) (Althorpe et al., 1999a; Bagdasarian et al., 1992; Bailone et
72 al., 1988; Dutreix et al., 1988) that inhibits SOS induction during conjugation (Baharoglu and Mazel,
73 2014; Baharoglu et al., 2010), and others proteins of unknown function. Remarkably, the leading
74 region is conserved in various enterobacterial plasmids belonging to a variety of incompatibility
75 groups (Cox and Schildbach, 2017; Golub and Low, 1985, 1986a; Golub et al., 1988; Loh et al., 1989,
76 1990). The adjacent and next transferred ~17 knt maintenance region carries the ParABS-like plasmid
77 partition system (SopABC) and the origins of vegetative replication (Bouet and Funnell, 2019;
78 Keasling et al., 1992; Kline, 1985; Thomas, 2000). The last transferred segment of the F plasmid is
79 the large ~33.3 knt *tra* region that encodes all the protein factors required for plasmid DNA processing
80 and transfer, including the relaxosome, the T4SS and the exclusion system against self-transfer
81 (Virolle et al., 2020). Besides, F plasmids often carry cargo genes involved in various metabolic
82 functions commonly integrated between the maintenance and the *tra* regions (Johnson et al., 2016;
83 Lanza et al., 2014).

84 Once both 5' and the 3' ends of the T-strand have been internalised into the recipient cell,
85 now called a transconjugant, the ssDNA plasmid is circularised by TraI and subsequently converted
86 into dsDNA by the complementary strand synthesis reaction (Chandler et al., 2013; Dostál and

87 Schildbach, 2010; Dostál et al., 2011; Draper et al., 2005; Garcillán-Barcia et al., 2007). The ss-to-
88 dsDNA conversion reaction is required for plasmid replication and partition and is, therefore, critical
89 to plasmid stability in the new host cell lineage.

90 The above-described mechanistic model is well-documented; however, the real time dynamics
91 and intracellular organisation of conjugation remain largely undescribed in the live bacterium. In
92 particular, we know very little about the subcellular localisation and timing of the reactions in the
93 recipient cell, including the ssDNA plasmid entry, the ss-to-dsDNA conversion and plasmid gene
94 expression. Regarding the latter, early works reported that some leading genes (*ssb^F* and *psiB* in F
95 plasmid, and *ssb^{Collb-P9}*, *psiB* and *ardA* in Collb-P9 plasmid) are expressed rapidly after entry of the
96 plasmid in the acceptor cell (Althorpe et al., 1999b; Bagdasarian et al., 1992; Cram et al., 1984;
97 Dutreix et al., 1988; Golub and Low, 1986a; Jones et al., 1992). *In vitro* work by Masai *et al.* (Masai
98 and Arai, 1997) showed that the single-stranded form of the non-coding *Frpo* sequence, located in
99 the F plasmid leading region, folds into a stem-loop structure that reconstitutes canonical -10 and -35
100 boxes. This promoter sequence can recruit the *E. coli* RNA polymerase that initiates RNA synthesis
101 in *in vitro* assays (Masai and Arai, 1997). Sequences homologous to *Frpo* were also found in the
102 leading region of Collb-P9 (Bates et al., 1999; Nasim et al., 2004). These observations led to the
103 proposal that *Frpo*-like sequences could act as ssDNA promoters initiating the early transcription of
104 leading genes when the plasmid is still in ssDNA form. Whether this regulation mechanism happens
105 during *in vivo* conjugation remains to be demonstrated.

106 In this study, we use live-cell microscopy imaging to visualise the complete transfer sequence
107 of the native F plasmid between *E. coli* K12 strains. We inspect the key steps of conjugation using
108 specifically developed genetic reporters, including a fluorescent fusion of the chromosomally
109 encoded single-strand-binding protein Ssb (Ssb-Ypet) to monitor the ssDNA transfer, the mCherry-
110 ParB/*parS* system to reveal the ss-to-dsDNA conversion and subsequent plasmid duplication, and
111 translational fluorescent fusions to quantify and time plasmid-encoded production in the new host
112 cell (Goldlust et al., 2022; Nolivos et al., 2019). This approach uncovers the choreography of

113 conjugation reactions in live bacteria and provides new insights into the interplay between plasmid
114 processing and gene expression.

115

116

117 **Results**

118 *Dynamics of the ssDNA plasmid during transfer*

119 We monitored the dynamic localisation of a fluorescent fusion of the chromosomally encoded single-
120 strand-binding protein Ssb (Ssb-Ypet) in donor and recipient cells, during vegetative growth and
121 conjugation (Figure 1A-B and Figure S1). During vegetative growth, Ssb-Ypet forms discrete foci at
122 midcell and quarter positions within the inner region of donors and recipient cells (Figure 1C and
123 Figure S2A-B). These Ssb foci, termed Ssb replicative foci hereafter, are associated with the ssDNA
124 that follows the replication forks onto the nucleoid DNA (Reyes-Lamothe et al., 2008, 2010). During
125 conjugation, the intracellular localisation of Ssb changes dramatically. As previously reported
126 (Goldlust et al., 2022; Nolivos et al., 2019), the entry of the ssDNA plasmid in the recipient cell, now
127 called a transconjugant, triggers the recruitment of Ssb molecules and the formation of bright
128 membrane-proximal foci, we termed Ssb conjugative foci (Figure 1B, Figure S1). Here, we also
129 observe the formation of Ssb conjugative foci in the donor cells, thus revealing the presence of ssDNA
130 plasmid on each side of the conjugation pore during transfer (Figure 1B, Figure S1). Foci localisation
131 analysis reveals that plasmid exit and entry occur at specific membrane positions within the mating
132 pair cells. Ssb conjugative foci are mainly distributed along the donor cells' side with a noticeable
133 enrichment at the cell quarter positions (Figure 1C, Figure S2A-B), reflecting the preferred position
134 for the exit of the ssDNA plasmid through active conjugation pores. By contrast, ssDNA plasmid
135 entry predominantly occurs within the polar regions of the transconjugant cells (Figure 1C, Figure
136 S2A-B). Our data also allow us to address whether conjugation occurs at a specific cell cycle stage.
137 Analysis of cell length as a proxy of cell age reveals that donor and recipient cells engaged in plasmid
138 transfer exhibit similar length distribution than during vegetative growth (Figure 1D). This shows

139 that conjugation is cell-cycle independent as the donors can give, and recipients can acquire the
140 plasmid at any stage of their cell cycle, from birth to cell division.

141 In $77.8 \pm 7\%$ ($n = 131$) of individual plasmid transfer events visualised by time-lapse imaging
142 (1 min/frame), Ssb conjugative foci appear in the donor and transconjugant cells on the same frame
143 (Figure 1E). In these cases, Ssb conjugative foci are, on average brighter in the transconjugant than
144 in the donor cells, reflecting the relative amount of ssDNA plasmid on each side of the conjugation
145 pore (Figure 1F). In the remaining 22.2 % of transfer events, Ssb conjugative foci first appear in the
146 transconjugant and then in the donor one or two minutes later (Figure 1E). The delayed accumulation
147 of ssDNA in the donor relative to the recipient is corroborated by the quantification of a 2.9 ± 1.1
148 min ($n = 294$) average lifespan of Ssb-Ypet conjugative foci in the transconjugants, compared to 2.5
149 ± 1.1 min ($n = 197$) in the donor cells (Figure 1G). These data indicate that the appearance of
150 conjugative foci is asynchronous in the mating pair cells and suggest a specific sequence of ssDNA
151 transfer. The first segment of the T-strand generated by the helicase activity of TraI in the donor cell
152 does not dwell long enough to recruit Ssb molecules and is immediately transferred to the recipient.
153 Only after this brief transfer stage does the ssDNA accumulates on the donor's side as well, where it
154 can correspond to either or both the non-transferred plasmid strand or to the T-strand. This implies
155 that the rate of ssDNA formation by TraI helicase activity is faster than that of ssDNA removal by
156 the RCR and transfer through the T4SS (See discussion).

157 The internalisation of a large amount of ssDNA plasmid provokes the massive recruitment of
158 the intracellular pool of Ssb molecules at the periphery of the donor and transconjugant cells. This
159 change in Ssb-Ypet subcellular distribution is revealed by skewness analysis, which provides a non-
160 biased measure of the asymmetry of fluorescence distribution within the cells without a requirement
161 for threshold-based foci detection (Figure 1H). Cells producing a free mCherry (mCh) exhibit a low
162 skewness corresponding to the homogeneous pixel fluorescence distribution inside the cell's
163 cytoplasm. During vegetative growth, Ssb-Ypet fluorescence is partly diffuse in the cytoplasm and
164 partly locally concentrated within replicative foci, resulting in a skewness of ~ 1.2 . By comparison,

165 Ssb-Ypet exhibits a strong skewness of ~ 4.1 in donors and transconjugants during plasmid transfer,
166 reflecting the increased proportion of Ssb molecules clustered within foci. Hence, we wondered what
167 part of Ssb molecules are contained within conjugative foci and if their formation was associated with
168 a depletion of Ssb within replicative foci in the transconjugant cell. To address this question, we
169 performed Ssb-Ypet foci automatic detection and brightness quantification during plasmid transfer
170 (Figure 1I). We observe that one minute after the beginning of plasmid entry Ssb-Ypet replicative
171 foci are still present but exhibit half their initial intensity, while conjugative foci are 35 times brighter.
172 Since the total Ssb-Ypet intracellular fluorescence is unchanged during the transfer (Figure S2C),
173 these variations can be attributable to the displacement of Ssb-Ypet molecules onto the incoming
174 ssDNA plasmid rather than Ssb-Ypet *de novo* synthesis. This dynamic reflects that the incoming
175 ssDNA plasmid recruits most Ssb-Ypet molecules in the acceptor cell during transfer.

176 It has been estimated that Ssb is present at about $\sim 1320 \pm 420$ monomers per *E. coli* cell and
177 that a dimer of tetramers covers about 170 nt *in vivo* (Reyes-Lamothe et al., 2010). Consequently,
178 there are not enough Ssb copies per cell to accommodate the 108 000 nucleotides ssDNA F plasmid,
179 plus the few hundreds of nucleotides of ssDNA associated with replication forks (~ 650 nt at 22°C
180 (Lohman and Ferrari, 1994)). This raises the possibility that the reduced availability of Ssb molecules
181 during plasmid entry could provoke a transitory disturbance of the host chromosome DNA
182 replication. One way to address this question *in vivo* is to monitor a fluorescent fusion of the β_2 -clamp
183 replisome component (mCh-DnaN), which is diffuse in the cytoplasm of non-replicating cells and
184 forms discrete replisome-associated foci during DNA replication progression (Moolman et al., 2014;
185 Reyes-Lamothe et al., 2008, 2010). Microscopy imaging and skewness analysis showed no change
186 in DnaN localisation pattern before, during or after Ssb conjugative foci formation (Figure S2D). This
187 indicates that Ssb recruitment onto the incoming ssDNA plasmid does not result in the collapse of
188 the replication fork. Whether the rate of DNA replication is affected during this transient and short
189 process remains a possibility.

190

191 ***ss-to-dsDNA conversion and subsequent plasmid replication in the transconjugant cells***

192 The conversion of the newly acquired ssDNA plasmid into dsDNA by the complementary strand
193 synthesis reaction and the subsequent plasmid duplication events were analysed using the *parS*/ParB
194 DNA labelling system (Goldlust et al., 2022; Nolivos et al., 2019). The *parS* binding site is inserted
195 in the F plasmid, while the ParB binding protein fluorescently labelled with the mCherry (mCh-ParB)
196 is produced from a plasmid in recipient cells only. Under the microscope, the ss-to-dsDNA
197 conversion is reported by the disappearance of the Ssb-Ypet conjugative focus and the formation of
198 a mCh-ParB focus in the transconjugant cells (Figure 2A). We first performed time-lapse imaging (1
199 min/frame) to visualise the success rate and timing of ss-to-dsDNA conversion after ssDNA entry
200 (Figure 2B). Analysis shows that the appearance of the Ssb-Ypet conjugative focus is followed by
201 the formation of the mCh-ParB focus in 83.3 ± 2.3 % ($n = 311$) individual transconjugant cells
202 analysed, indicating that the vast majority of internalised ssDNA plasmids are successfully converted
203 into dsDNA plasmids (Figure 2C). Notably, we observe that 40 ± 3.2 % ($n = 286$) of transconjugant
204 cells where the newly acquired ssDNA plasmid has already been converted into dsDNA subsequently
205 receive additional ssDNA (Figure 2D, Figure S3A). We quantify that 92 ± 3.1 % of these multiple
206 ssDNA acquisition events originate from the same donor, among which 79 ± 5.3 % appear to take
207 place at the same membrane position, suggesting that they occur through the same conjugation pore
208 (Figure S3A). The evidence for multiple transfers within an established mating pair demonstrates that
209 a single donor can successively give several copies of the T-strand and that transconjugants in which
210 the ss-to-dsDNA conversion has already been achieved do not become instantly refractory to *de novo*
211 plasmid acquisition. Accordingly, establishing immunity to conjugation by transconjugant cells is
212 expected to require the production of the plasmid-encoded exclusion proteins TraS and TraT.

213 Considering successful ss-to-dsDNA events only, we calculate an average 4 ± 1.6 min ($n =$
214 475) time lag between the appearance of the Ssb-Ypet conjugative focus and the formation of the
215 mCh-ParB focus (Figure 2E). This period reflects the time required for the completion of a reaction
216 cascade that comprises the complete internalisation of the ssDNA plasmid, the circularisation of the

217 ssDNA plasmid by TraI, the initiation and completion of the complementary strand synthesis
218 replication, and the recruitment of ParB molecules on the *parS* site in dsDNA form. Though our
219 system does not allow evaluating each step's contribution, results show that the complete sequence
220 of reactions is achieved within a relatively short and consistent period.

221 Next, we first performed time-lapse imaging (5 min/frame) to examine the timing of plasmid
222 duplication in transconjugant cells (*i.e.*, replication and visual separation of the plasmid copies)
223 (Figure 2B). We estimate an average of 10.4 ± 4.7 min ($n = 158$) period between the ssDNA-to-
224 dsDNA conversion and the first plasmid duplication event (from one to two mCh-ParB foci) and
225 similar 10.1 ± 5.1 min ($n = 124$) between the first and the second duplication event (from two to three
226 or four mCh-ParB foci) (Figure 2F). We then decided to compare the rate of plasmid duplication in
227 transconjugants to the rate of plasmid duplication in a vegetatively growing F-carrying donor strain.
228 To do so, we plotted the number of plasmid foci per cell from the ss-to-dsDNA conversion (mCh
229 focus appearance) to cell division in transconjugants and from cell birth to cell division in F-carrying
230 donor cells (Figure 2G). Results show that the number of F per cell increases significantly faster in
231 transconjugant cells than in vegetatively growing F-carrying cells (75 % increase of the fit curve
232 slope), yet to reach a similar final number of $\sim 4 \pm 1$ copies per cell before division (Figure 2G). F
233 copy number, like chromosome replication, is known to be controlled by the cell cycle progression,
234 where initiation occurs when a constant mass per origin is achieved (Keasling et al., 1991). Therefore,
235 our observations are consistent with the interpretation that when a single plasmid copy arrives in a
236 recipient cell that can be at any cell cycle stage, plasmid replication initiation is unrepressed until the
237 specific number of plasmid copies per cell mass is restored. This accelerated plasmid replication
238 allows for the rapid increase in F copy number before the division of the transconjugant cells, thus
239 facilitating the segregation of plasmid copies to daughter cells.

240 Localisation analysis reveals that the ss-to-dsDNA conversion and the first duplication event
241 occur at distinct subcellular positions. The initial mCh-ParB focus preferentially appears in the polar
242 region of the transconjugant cell, comparable to the ssDNA's entry location (compare Figure 2H to

243 Figure 1C and Figure S3B to Figure S2A). A noticeable difference is that mCh-ParB foci appear less
244 peripheral, indicating that they are not as close to the cell membrane as Ssb-Ypet conjugation foci
245 (compare Figure 2H to Figure 1C, and Figure S3C to Figure S2B). We observe that the mCh-ParB
246 focus subsequently migrates to the midcell position before duplication (Figure 2H, Figure S3B-C).
247 These data show that the two DNA synthesis reactions involved in plasmid processing (*i.e.*, ss-to-
248 dsDNA conversion and plasmid replication) are separated in time and space in the new host cell. The
249 recruitment of the complementary strand synthesis machinery and the ss-to-dsDNA replication
250 reaction occur in the vicinity of the polar position of entry of the ssDNA plasmid, while plasmid
251 replication occurs in the midcell region. Altogether, these analyses reveal that plasmid processing
252 steps (ssDNA entry, ss-to-dsDNA conversion and plasmid replication) occur at specific intracellular
253 positions within the new host cell and follow a precise chronology.

254

255 ***Program of plasmid-encoded protein production in transconjugant cells***

256 We constructed *superfolder gfp* (*sfgfp*) C-terminal translational fusions to several genes located in
257 the different functional regions of the F plasmid to examine the production timing of plasmid-encoded
258 proteins in transconjugant cells, which we use to get insights into the timing of plasmid gene
259 expression (Figure 3A, Figure S4A). *YgfA*, *ygeA*, *psiB*, *yfjB*, *yfjA* and *ssb^F* are located in the leading
260 region and are transferred in order after the origin of transfer *oriT*. The *sopB* gene is part of the
261 SopABC partition system and is located in the maintenance region. The *traM*, *traC*, *traS* and *traT*
262 genes are located in the *tra* region that encodes factors involved in plasmid transfer. TraM is the
263 accessory protein of the relaxosome complex that is recruited to the *oriT* (Di Laurenzio et al., 1992);
264 TraC is the traffic ATPase organised as a hexamer of dimers docked to the cytoplasmic faces of the
265 T4SS (Hu et al., 2019); TraS and TraT correspond to the F plasmid exclusion (immunity) system that
266 protects against self-transfer (Achtman et al., 1977; Jalajakumari et al., 1987; Manning et al., 1980).

267 We first performed time-course experiments where microscopy snapshot images of the
268 conjugating population were acquired 1, 2, 4 and 6 hours after mixing donors and recipient cells. For

269 each time point, the frequency of transconjugants (T/R+T) was directly measured at the single-cell
270 level from the proportion of recipient cells exhibiting diffuse mCh-ParB fluorescence (R) or
271 transconjugant cells harbouring mCh-ParB foci (T), and the intracellular green fluorescence Signal
272 to Noise Ratio (SNR) was automatically measured (Figure S4B-D). This snapshot analysis shows
273 that all F plasmid derivatives carrying sfGFP fusions retained their transfer ability and raised
274 frequencies of transconjugants between 57 and 93 % after 6 hours of mating. Also, fusion-carrying
275 plasmid acquisition is systematically followed by an increase in sfGFP signal in transconjugant cells,
276 with highly variable timing and levels (Figure S4B-D).

277 Better resolution of the production level and timing of sfGFP fusions with respect to the ss-
278 to-dsDNA conversion (appearance of the mCh-ParB focus) in individual transconjugant cells was
279 obtained using time-lapse imaging of conjugation performed in the microfluidic chamber (Movie S1
280 and S2). We performed transconjugant cell detection and quantification of the intracellular sfGFP
281 SNR cells over time (Figure S5A-D). When the transconjugant cell divided, we continued
282 fluorescence quantification in the resulting daughter cells to monitor sfGFP production over a longer
283 period. From this raw data, we calculated the fold-increase in SNR per ten-minute interval, where a
284 fold-increase superior to one reveals that the fusions are being produced in the transconjugants
285 (Figure S5A-D). These data were finally translated into a comprehensive diagram presenting the
286 production time windows for each fusion in transconjugant cells relative to the ss-to-dsDNA
287 conversion event (Figure 3B). This analysis reveals that fusions belonging to the different plasmid
288 regions exhibit specific production timings with respect to plasmid processing steps.

289 Remarkably, we detect the synchronous production of the leading YgeA, PsiB, YfjB, YfjA
290 and Ssb^F fusion proteins even before the appearance of the mCh-ParB focus (Figure 3B and Figure
291 S5A). Furthermore, the production of these fusions is only transient as it peaks at ~5 minutes and
292 stops 25-35 minutes after the ss-to-dsDNA conversion event. This unexpected observation indicates
293 that leading fusions start being produced when the plasmid is still in ssDNA form and stops rapidly
294 after the plasmid is converted into dsDNA form. An interesting exception is YgfA-sfGFP, for which

295 production is only detected in the 10-20 minutes interval after mCh-ParB focus appearance. The *ygfA*
296 gene is the closest to the *oriT* and is, therefore, the first gene to be transferred into the recipient (Figure
297 3A, Figure S4A). However, *ygfA* gene orientation is opposite to other tested leading genes, meaning
298 that the T-strand does not correspond to the template strand for *ygfA* transcription. Consequently, and
299 consistent with our observations, *ygfA* expression can only occur after synthesising the
300 complementary template strand by the ss-to-dsDNA conversion.

301 The ss-to-dsDNA conversion is followed by the production of maintenance and Tra proteins,
302 starting with SopB and TraM, then TraC, and eventually TraS and TraT fusions (Figure 3B, Figure
303 S5B-C). The production of these fusions is expected to require the presence of the plasmid in dsDNA
304 form since the corresponding genes are known to be controlled by dsDNA promoters (P_{sopAB} for *sopB*,
305 P_M for *traM* and P_Y for *traC* and *traST*). However, what could explain the observed differences in the
306 production timings? We addressed whether timing discrepancies could simply account for the
307 fusions' position on the genetic map of the F plasmid. This possibility was excluded by the
308 observation that insertion of the constitutive fluorescent reporter P_{lacIQ1} sfGFP (*sfgfp* gene under the
309 control of the P_{lacIQ1} constitutive promoter) in the *repE-sopA*, *tnpA-ybaA* and *traM-traJ* intergenic
310 regions resulted in similar sfGFP production timings, within the 0-10 minutes interval after the
311 appearance of the mCh-ParB focus (Figure 3B, Figure S5D). Instead, we propose that the differential
312 production timings of maintenance and *tra* genes reflect the activity and regulation of the promoters
313 of the corresponding genes. The *sopAB* operon is under the control of the P_{sopAB} promoter, which is
314 repressed by SopA binding. Therefore, the P_{sopAB} promoter is expected to be fully unrepressed and
315 active in transconjugant cells devoid of SopA, thus allowing the rapid production of the SopAB
316 partition complex required for plasmid stability and inheritance over cell divisions. The *traM* gene is
317 controlled by the P_M promoter, which is weakly but constitutively active, even before its full
318 activation by binding the TraY protein (Penfold et al., 1996). By contrast, the P_Y promoter that
319 controls the expression of *traC*, *traS* and *traT* genes needs to be activated by the TraJ protein, encoded
320 by the *traJ* gene under the control of its own promoter P_J and located upstream of P_Y (Virolle et al.,

321 2020). The requirement for this activation cascade probably explains the delayed production of TraC,
322 TraS and TraT. The additional delay between TraC and TraS/TraT fusions production could
323 potentially reflect the relative distance of these genes to the *P_Y* promoter (5.9 kb for *traC* and 20.4 kb
324 for *traST*).

325 Notably, the intracellular levels of Tra proteins within transconjugant cells reach a plateau
326 between 60 to 90 minutes after the ss-to-dsDNA conversion and remain stable throughout our
327 observations (Figure 3B, Figure S5C). This involves that at that point, transconjugant cells have
328 produced the transfer machinery and the exclusion system and have most likely been converted into
329 proficient plasmid donors. In support of this interpretation, TraM, TraC, TraS, TraT and SopB are
330 detected at similar levels in vegetatively growing F-carrying donor cells (Figure 3C, Figure S4C-D
331 and S5B-C). This is not the case for YgeA, PsiB, YfjB, YfjA, and Ssb^F leading proteins, which
332 intracellular levels start decreasing 25-35 minutes after the ss-to-dsDNA conversion in the
333 transconjugants, and which are not detected in vegetatively growing donor cells (Figure 3C, Figure
334 S4B and S5A). These results are consistent with the interpretation that leading proteins are produced
335 rapidly and only transiently upon entry of the ssDNA plasmid in the recipient cells and not when the
336 plasmid is maintained in dsDNA form during vegetative replication.

337

338 ***Single-stranded promoters allow the early expression of the leading genes in the transconjugant*** 339 ***cell***

340 Together with previous works (Althorpe et al., 1999b; Bagdasarian et al., 1992; Bates et al., 1999;
341 Jones et al., 1992), the early and transiently expression of leading genes in transconjugant cells
342 support the existence of specific sequences that would act as single-stranded promoters to initiate the
343 transcription of leading genes from the internalised ssDNA plasmid. Using bioinformatics analysis,
344 we identified a region upstream of the *ssb^F*, *yfjA*, *yfjB*, *psiA* and *psiB* genes, which we named *Frpo2*,
345 that shares 92% identity with the previously reported *Frpo* region (renamed *Frpo1*) located upstream
346 *ygeA* and *ygeB* and previously characterised *in vitro* (Masai and Arai, 1997) (Figure 4A). DNA

347 folding prediction using mFold (<http://www.unafold.org>) indicates that the single-stranded form of
348 *Frpo2* can fold into a highly stable stem-loop structure that also carries canonical -10 and -35 boxes,
349 similar to the *Frpo1* region (Figure S6A) (Masai and Arai, 1997). We addressed the effect of *Frpo1*
350 or *Frpo2* deletions on the expression of the downstream genes in transconjugant cells using live-cell
351 microscopy. Microscopy analysis of transconjugant cells receiving the F Δ *Frpo1* *ygeA-sfgfp*, the F
352 Δ *Frpo2* *ssb^F-sfgfp*, or the F Δ *Frpo2* *yjfa-sfgfp* revealed no significant fold-increase in sfGFP
353 fluorescence before or after the ss-to-dsDNA conversion in the transconjugant cells (Figure 4B).

354 We then addressed the impact of *Frpo1* and *Frpo2* deletions on the efficiency of conjugation
355 after three hours of mating, as estimated by plating assays (Figure 4C). F Δ *Frpo1* exhibits a
356 dramatically reduced frequency of transconjugants of 25.2 ± 2.9 % compared to 92.6 ± 6.6 % for the
357 *Fwt*. Comparable results were obtained for F Δ *Frpo1* Δ *ygeAB* (32.7 ± 7.1) and F Δ *Frpo1* Δ *ygeA* (14.5
358 ± 0.4). Surprisingly, the single deletion of *ygeA* decreases the conjugation of efficiency even further
359 (3.9 ± 1.9 %), and despite our multiple attempts, the deletion of *ygeB* alone could never be
360 constructed. By contrast, the deletions of *Frpo2* or *ssb^F* have no significant impact on the conjugation
361 efficiency. These results show that *Frpo1* and *Frpo2* are required for the early expression of the
362 downstream genes upon plasmid entry in recipient cells during conjugation *in vivo*. However, genes
363 under the control of *Frpo1* appear to have a more critical role in conjugation than those under the
364 control of *Frpo2*.

365

366 ***Role of the plasmid-encoded Ssb^F leading protein in plasmid establishment***

367 The rapid and transient expression of leading genes upon plasmid entry strongly suggests that leading
368 proteins have an essential role during the early steps of plasmid establishment in the new host cell.
369 The leading region conserved in various enterobacterial plasmids encodes a homolog of the single-
370 strand-binding protein Ssb encoded on the *E. coli* chromosome (Golub and Low, 1985, 1986b; Golub
371 et al., 1988; Howland et al., 1989; Jones et al., 1992; Kolodkin et al., 1983). The chromosomally
372 encoded *ssb* gene is conserved and essential in all bacterial organisms, raising the question of the

373 *raison d'être* of plasmid-born *ssb* homologues. Early study shows that the Ssb^F encoded by the F
374 plasmid can partially complement conditional mutations of the chromosomal *ssb* gene (Golub and
375 Low, 1986b; Porter and Black, 1991). Consistently, we performed simultaneous visualisation of Ssb^F-
376 mCh produced from a pTrc99a-*ssb*^F-*mch* plasmid and the chromosomally-encoded Ssb-Ypet (Figure
377 S7A) and observed similar intracellular positioning (Figure S7B) confirmed by colocalisation
378 analysis (Figure S7C). This indicates that both the plasmid Ssb^F and the host Ssb are recruited to the
379 ssDNA that follows the replication forks in vegetatively growing cells. Similarly, Ssb^F-sfGFP also
380 forms foci in transconjugant cells that have acquired the F *ssb*^F-*sfGFP* plasmid, mainly during the first
381 and second plasmid duplication events (Figure S7D-E). Nonetheless, the role of Ssb^F during
382 conjugation is still unclear, and its deletion from the F plasmid has no significant impact on
383 conjugation efficiency (Figure 4C).

384 To get further insight into the role of Ssb^F during conjugation, we revisited the dynamics of
385 ssDNA entry, ss-to-dsDNA conversion and duplication of the F Δ *ssb*^F plasmid. Time-lapse
386 microscopy image analysis reveals that Ssb^F deletion has no impact on the dynamics of Ssb-Ypet
387 conjugative foci (Figure 4D) or the timing of the ss-to-dsDNA conversion (compare Figure 4E to
388 Figure 2E). However, Ssb^F deletion dramatically delays the timing of plasmid duplication in
389 transconjugant cells (compare Figure 4F to Figure 2F). The time lag between mCh-ParB appearance
390 and the first duplication is increased by ~58 % (from 10.4 ± 4.7 for F_{wt} to 16.4 ± 9.5 for F Δ *ssb*^F),
391 and the time between the first and second plasmid replication event is increased by ~29 % (from 10.1
392 ± 4.7 for F_{wt} to 13 ± 8 for F Δ *ssb*^F). This indicates that Ssb^F has a role in facilitating the first rounds
393 of plasmid duplication in the new transconjugant cell, possibly by increasing the cellular pool of
394 single-strand binding protein available for DNA replication. This function appears dispensable since
395 the absence of Ssb^F delays plasmid duplication but does not affect the final efficiency of conjugation,
396 at least when conjugation is performed in optimal conditions between *E. coli* MG1655 strains.

397

398

399 **Discussion**

400 Our current knowledge of conjugation mainly emerges from experimental genetic, biochemical and
401 structural studies that provided a well-documented understanding of the molecular reactions and
402 factors involved in DNA transfer, while genomic and computational studies uncovered the diversity
403 of conjugative plasmids and their importance in the epidemiology of antibiotics resistance
404 dissemination. It is only recently that the application of optical microscopy has started to provide
405 insights into the organisation of conjugation at the cellular scale (Aguilar et al., 2011; Babic et al.,
406 2011; Babić et al., 2008; Carranza et al., 2021; Clarke et al., 2008; Goldlust et al., 2022; Lawley et
407 al., 2002; Low et al., 2022; Nolivos et al., 2019). In this study, live-cell microscopy combined with
408 specifically developed fluorescent reporters offers a unique view of the cellular dynamics of
409 conjugation while providing insights into the timing and localisation of each key step.

410 We report the presence of ssDNA plasmid on both the donor and the recipient's side during
411 plasmid transfer. Noticeably, the ssDNA plasmid is not randomly positioned but instead allocated to
412 specific subcellular locations within the mating pair cells. The exit point of the ssDNA is
413 preferentially located on the side of the donor cell and enriched at quarter positions. This unlikely
414 reflects a specific positioning of the T4SS machinery, which was reported to be homogeneously
415 located throughout the periphery of the cells (Aguilar et al., 2011; Carranza et al., 2021). Instead, the
416 observed lateral localisation of active conjugation pores may reflect the facilitated access to F plasmid
417 molecules, which are also positioned at quarter positions and excluded from the cell poles (Gordon
418 et al., 2004; Niki and Hiraga, 1997). By contrast, the ssDNA mainly enters the polar region of the
419 recipient cells. This could suggest that the pole of the recipients' surface is the preferred location for
420 the donor's F-pilus attachment or the stabilisation of the mating pair. The latter possibility is
421 reinforced by the fact that mating pair stabilisation during F conjugation involves interaction between
422 the plasmid protein TraN exposed at the surface of the donor cells and the host outer membrane
423 protein OmpA of the recipient cells (Klimke and Frost, 1998; Low et al., 2022). OmpA was shown

424 to be enriched and less mobile in the polar regions of *E. coli* cells (Verhoeven et al., 2013), possibly
425 favouring the stabilisation of the mating pair and the conjugation pore at this location.

426 The unexpected finding that the ssDNA is present in the donor during conjugation also
427 provides insights into the activity of TraI and its coordination with the transfer of the T-strand through
428 the T4SS or the RCR of the non-transferred strand. Before DNA transfer initiation, the relaxosome
429 bound to the plasmid's *oriT* is docked to the T4SS by the TraD (VirD4) coupling protein, thus forming
430 the pre-initiation complex (Figure 5A(i)). Contact with the recipient cell is proposed to induce a signal
431 that activates the pre-initiation complex. We uncover the existence of a brief stage where part of the
432 T-strand has already been transferred into the recipient cell while no ssDNA is present within the
433 donor (Figure 5A(ii)). At this stage, the absence of ssDNA in the donor implicates that all the ssDNA
434 generated by TraI has been removed, both by transfer of the T-strand through the T4SS and by
435 complementation of the non-transferred ssDNA strand by the RCR. After this transient stage, the
436 ssDNA also accumulates in the donor, suggesting that the ssDNA is generated by TraI helicase
437 activity in the donor faster than it is removed by transfer and RCR synthesis (Figure 5A(iii)).

438 Assuming the 2.9 ± 1.1 min lifespan of the Ssb-Ypet foci in transconjugants reflects the time
439 required to complete the internalisation of the 108 000 nt ssDNA F plasmid, we calculated a $620 \pm$
440 $164 \text{ nt}\cdot\text{s}^{-1}$ transfer rate. This is in reasonable agreement with the historical $770 \text{ nt}\cdot\text{s}^{-1}$ rate estimated
441 from the 100 minutes required to transfer the whole 4.6 Mb *E. coli* chromosome (Jacob and Wollman,
442 1958). Besides, the rate of DNA synthesis by the DNA polymerase III holoenzyme during RCR was
443 estimated at $650\text{-}750 \text{ nuc}\cdot\text{s}^{-1}$ (Stephens and McMacken, 1997). By comparison, the rate of TraI
444 helicase activity was measured at $1120 \pm 160 \text{ bp}\cdot\text{s}^{-1}$ (Sikora et al., 2006). These estimates support the
445 view that ssDNA accumulation in the donor accounts for the faster rate of TraI helicase activity than
446 the rate of T-strand plasmid transfer or RCR. Therefore, it is possible that, contrasting with the
447 previously suggested but never demonstrated proposal, the helicase activity of the relaxase is not
448 strictly coupled with the activity of DNA translocation through the T4SS.

449 Live-cell microscopy uncovers the global chronology conjugation steps, as summarised in
450 Figure 5B. The plasmid processing in the transconjugant cell is a relatively rapid process, as the entry
451 of the ssDNA plasmid and its conversion into dsDNA is completed in about 4 minutes on average.
452 Most importantly, the ss-to-dsDNA conversion event is the pivotal event that determines the program
453 of plasmid gene expression. Leading genes are the first to enter the recipient cell and also the first to
454 be expressed from the F plasmid in ssDNA form. Consistently with previous proposals (Bates et al.,
455 1999; Masai and Arai, 1997; Nasim et al., 2004), we show that the early expression of leading genes
456 depends on sequences that act as single-stranded promoters when the plasmid is still in ssDNA form.
457 As previously described for *Frp01*, we propose that the highly homologous *Frp02* sequences
458 identified here folds into a stable stem-loop structures that reconstruct -35 and -10 consensus boxes,
459 resulting in transcription initiation.

460 Leading gene expression is also transient as the ss-to-dsDNA conversion turns off leading
461 protein production by inactivating *Frp01* and *Frp02* promoters while licencing the expression of
462 maintenance, transfer and other plasmid genes under the control of conventional dsDNA promoters,
463 often subject to their own regulation specificities. Maintenance and transfer protein levels within
464 transconjugants reach a steady-state equivalent to that of vegetatively growing F-containing cells in
465 about 30 to 90 minutes, depending on the protein. Interestingly, our previous work showed that
466 tetracycline resistance factors encoded by the *Tn10* transposon inserted in the intergenic region *ybdB*-
467 *ybfA* of the F plasmid are also produced immediately after the ss-to-dsDNA conversion and reach the
468 resistant cell's level within approximately 90 minutes (Nolivos et al., 2019). These findings
469 consistently indicate that this time scale corresponds to the period needed for the transconjugant cells
470 to gain plasmid-encoded functions, including plasmid maintenance, conjugation ability, immunity
471 against self-transfer and additional resistance potentially carried by the plasmid.

472 The regulation of plasmid gene expression by plasmid processing is an elegant way to ensure
473 the sequential and timely production of plasmid proteins in the transconjugant cell, and particularly
474 to restrict the production of leading factors to a narrow time window following the entry of the ssDNA

475 plasmid. However, *de novo* protein synthesis might not be the only way to provide the transconjugant
476 cell with plasmid-encoded proteins. Recent work by Al Mamun *et al.* reports that the transfer of the
477 F-like plasmid pED208 (IncFV) is concomitant with the translocation of several plasmid-encoded
478 proteins, including TraI, ParA, ParB1, Ssb homologue Ssb^{ED208}, ParB2, PsiB, and PsiA (Al Mamun
479 *et al.*, 2021). Protein translocation was detected at low frequency (10^{-5} recombinants per donor cell
480 between one and five hours of mating) using a highly sensitive Cre recombinase assay. Protein
481 translocation might also occur during the transfer of the native F plasmid but could not solely explain
482 our observations. Indeed, our microscopy analysis shows that YgeA, PsiB, YfjB, YfjA and Ssb^F
483 leading fusions are below the microscopy detection threshold in donor cells but are quantified at
484 significant intracellular levels in all transconjugant cells. This implies that the amounts of leading
485 proteins observed in the transconjugant cells cannot just originate from donor cells, but result from
486 *de novo* protein synthesis, which we show depends on *Frpo1* and *Frpo2* sequences.

487 Both the early production and the direct translocation of leading proteins suggest a critical
488 role of the leading region in conjugation. Several elements support this view. The leading region is
489 conserved in a variety of conjugative plasmids (Cox and Schildbach, 2017; Golub and Low, 1985,
490 1986a; Golub *et al.*, 1988; Loh *et al.*, 1989, 1990). In addition, the leading regions of plasmids
491 belonging to a wide range of incompatibility groups (IncF, IncN, IncP9 and IncW) classified as
492 MOBF plasmids using the relaxase as a phylogenetic marker were reported to be the preferential
493 target for CRISPR-Cas systems directed against conjugation (Fernandez-Lopez *et al.*, 2016;
494 Garcillán-Barcia *et al.*, 2009; Westra *et al.*, 2013). Recently, the leading region was shown to be an
495 important evolutionary target for the dissemination of the pESLB (IncI) plasmid (Benz and Hall,
496 2022). Concerning the F plasmid, we can stress that *Frpo1* and *Frpo2* share 92 % similarity at the
497 nucleotide level and are located only about 5 kb apart. This implies that when in dsDNA form during
498 vegetative plasmid replication, *Frpo1* and *Frpo2* sequences would be a potential substrate for
499 homologous recombination, resulting in the deletion of the intervening segment. However, the
500 intervening segment carries the *flmAB* genes, functional homologues to the *hok/sok* toxin-antitoxin

501 system from the R1 plasmid (Loh et al., 1988), which are likely to safeguard the stability of the
502 leading region.

503 Despite this body of evidence, it is currently challenging to rationalise the importance of the
504 leading region since the molecular functions of most leading proteins are still unknown. Our data
505 indicate that genes downstream of *Frpo1* (*ygeA* et *ygeB*) have a critical function in conjugation. By
506 contrast, genes located downstream *Frpo2* (*ssb^F*, *yjjA*, *yjjB*, *psiB*, *psiA* and *flmC*) appear to be
507 dispensable since deletions of *Frpo2*, *ssb^F* or *psiB* (Loh et al., 1989) have no significant impact on
508 the overall conjugation efficiency addressed by plating assays. However, conjugation efficiency
509 assays are generally performed between identical or closely related bacterial strains in optimal
510 medium and temperature conditions. This likely undermines the role of genes that are not strictly
511 essential but might facilitate or optimise conjugation. Hence, it is possible that the importance of the
512 leading factors would be best revealed in less favourable conditions, between phylogenetically distant
513 bacteria, or on the evolutionary scale. Meanwhile, real time microscopy might help uncover the
514 potentially subtle influence of these genes on the sequence of conjugation in live cells.

515

516

517 **Acknowledgements**

518 The authors thank the National BioResource Project and Coli Genetic Stock Center for providing
519 strains, A. Ducret for valuable help with MicrobeJ and N. Fraikin for helpful discussion. **Funding:**

520 This research was funded by the Foundation for Medical Research, grant number FRM-

521 EQU202103012587 to C.L. and A.C.; the French National Research Agency, grant number ANR-18-

522 CE35-0008 to C.L., Y.Y., and K. G.; and the University of Lyon through funding to C.V. C.L. also

523 acknowledges the Schlumberger Foundation for Education and Research (FSER 2019). **Author**

524 **contributions:** C.L. and S.B. conceived, designed and supervised the execution of the study; A.C.,

525 C.V., K.G., A.R., S.N. and S.B. performed the experiments and analysed the data. C.L. and S.B. wrote

526 the paper, and C. L. prepared the figures. C.L. and Y.Y. provided funding. **Competing Financial**

527 **Interests:** The authors declare no competing financial interests. **Data and materials availability:**
528 All data to understand and assess the conclusions of this research are available in the main text and
529 Supplementary Materials.

530

531

532 **Materials and Methods**

533 **Bacterial strains, plasmids and growth**

534 Bacterial strains are listed in Table S1, plasmids in Table S2, and oligonucleotides in Tables S3.
535 Fusion of genes with fluorescent tags and gene deletion on the F plasmid used λ Red recombination
536 (Datsenko and Wanner, 2000; Yu et al., 2000). Modified F plasmids were transferred to the
537 background strain K12 MG1655 by conjugation. Where multiple genetic modifications on the F
538 plasmid were required, the *kan* and *cat* genes were removed using site-specific recombination induced
539 by expression of the Flp recombinase from plasmid pCP20 (Datsenko and Wanner, 2000). Plasmid
540 cloning were done by Gibson Assembly and verified by Sanger sequencing (Eurofins Genomics
541 biotech). Strains and plasmids were verified by Sanger sequencing (Eurofins Genomics). Cells were
542 grown at 37°C in M9 medium supplemented with glucose (0.2 %) and casamino acid (0.4 %) (M9-
543 CASA) before imaging, and in Luria-Bertani (LB) broth for conjugation efficiency assays. When
544 appropriate, supplements were used in the following concentrations; Ampicillin (Ap) 100 μ g/ml,
545 Chloramphenicol (Cm) 20 μ g/ml, Kanamycin (Kn) 50 μ g/ml, Streptomycin (St) 20 μ g/ml, and
546 Tetracycline (Tc) 10 μ g/ml.

547

548 **Conjugation assays**

549 Overnight cultures in LB of recipient and donor cells were diluted to an A_{600} of 0.05 and grown until
550 an A_{600} comprised between 0.7 and 0.9 was reached. 25 μ l of donor and 75 μ l of recipient cultures
551 were mixed into an Eppendorf tube and incubated for 90 minutes at 37°C. 1 ml of LB was added
552 gently and the tubes were incubated again for 90 min at 37°C. Conjugation mix were vortexed, serial

553 diluted, and plated on LB agar X-gal 40 μ g/ml IPTG 20 μ M supplemented the appropriate antibiotic
554 to select for recipient or donor populations. Recipient (R) colonies were then streaked on plated on
555 LB agar containing tetracycline 10 μ g/ml to select for transconjugants (T) and the frequency of
556 transconjugant calculated from the (T/R+T) presented in Figure 4C.

557

558 **Live-cell microscopy experiments**

559 Overnight cultures in M9-CASA were diluted to an A_{600} of 0.05 and grown until $A_{600} = 0.8$ was
560 reached. Conjugation samples were obtained by mixing 25 μ l of donor and 75 μ l of recipient into an
561 Eppendorf tube. For time-lapse experiments, 50 μ l of the pure culture or conjugation mix was loaded
562 into a B04A microfluidic chamber (ONIX, CellASIC®) (Cayron and Lesterlin, 2019). Nutrient
563 supply was maintained at 1 psi and the temperature maintained at 37°C throughout the imaging
564 process. Cells were imaged every 1 or 5 min for 90 to 120 minutes. For snapshot imaging, 10 μ l
565 samples of clonal culture or conjugation mix were spotted onto an M9-CASA 1% agarose pad on a
566 slide (Lesterlin and Duabrry, 2016) and imaged directly.

567

568 *Image acquisition.* Conventional wide-field fluorescence microscopy imaging was carried out on an
569 Eclipse Ti2-E microscope (Nikon), equipped with x100/1.45 oil Plan Apo Lambda phase objective,
570 ORCA-Fusion digital CMOS camera (Hamamatsu), and using NIS software for image acquisition.
571 Acquisitions were performed using 50% power of a Fluo LED Spectra X light source at 488 nm and
572 560 nm excitation wavelengths. Exposure settings were 100 ms for Ypet, sfGFP and mCherry and 50
573 ms for phase contrast.

574 *Image analysis.* Quantitative image analysis was done using Fiji software with MicrobeJ plugin
575 (Ducret et al., 2016). For snapshot analysis, cells' outline detection was performed automatically
576 using MicrobeJ and verified using the Manual-editing interface. For time-lapse experiments,
577 detection of cells was done semi-automatedly using the Manual-editing interface, which allows to
578 select the cells to be monitored and automatically detect the cell outlines. Within conjugation

579 populations, donor (no mCh-ParB signal), recipient (diffuse mCh-ParB signal), or transconjugant
580 (mCh-ParB foci) category were assigned using the ‘Type’ option of MicrobeJ. Recipient cells were
581 detected on the basis of the presence of red fluorescence above the cell’s autofluorescence
582 background level detected in the donors. Among these recipient cells, transconjugants were identified
583 by running MicrobeJ automated detection of the ParB fluorescence foci (Maxima detection). This
584 approach was used independently of the presence or the absence of the Ssb-Ypet, or sfGFP fusions
585 within donor and recipient cells. Within the different cell types, mean intensity fluorescence (a.u.),
586 skewness, Signal/Noise Ratio (SNR), or cell length (μm) parameters were automatically extracted
587 and plotted using MicrobeJ. SNR corresponds to the ratio (mean intracellular signal / mean noise
588 signal), where the mean intracellular signal is the fluorescence signal per cell area and the noise is
589 the signal measured outside the cells (due to the fluorescence emitted by the surrounding medium).
590 By contrast with the total amount of fluorescence per cell, which is depending on the cell size/age
591 and accounts for the background, SNR quantitative estimate is more appropriate for unbiased
592 quantification of intracellular fluorescence over time. Ssb-Ypet, Ssb^F-mCh and mCh-ParB foci were
593 detected using MicrobeJ Maxima detection function, and foci localisation and fluorescence intensity
594 were extracted and plotted automatically. Plots presenting time-lapse data were either aligned to the
595 first frame where the transconjugant cell exhibits a conjugative Ssb-Ypet focus (ssDNA acquisition)
596 or a mCh-ParB focus (ss-to-dsDNA conversion) as indicated in the corresponding figure legend.

597

598 **Statistical analysis**

599 *P*-value significance were analysed running specific statistical tests on the GraphPad Prism software.
600 Single-cell data from quantitative microscopy analysis were extracted from the MicrobeJ interface
601 and transferred to GraphPad. *P*-value significance of single-cell quantitative data was performed
602 using unpaired non-parametric Mann-Whitney statistical test, which allows to compare differences
603 between independent data groups without normal distribution assumption. *P*-value significance for
604 the frequency of transconjugants obtained by plating assays were evaluated using One-way analysis

605 of variance (ANOVA) with Dunnetts multiple comparisons test, which allows to determine the
606 statistical significant of differences observed between the means of three or more independent
607 experimental groups against a control group mean (corresponding to the *Fwt*). When required, *P*-
608 value and significance are indicated on the figure panels and within the corresponding legend.

609

610

611 **SUPPLEMENTARY MATERIALS**

612 Figs. S1 to S7

613 Tables S1 to S3

614 Captions for Movies S1 to S3

615 Movies S1 to S3

616 **References**

- 617 Achtman, M., Kennedy, N., and Skurray, R. (1977). Cell-cell interactions in conjugating
618 *Escherichia coli*: role of traT protein in surface exclusion. *Proc Natl Acad Sci U S A* 74, 5104–
619 5108. .
- 620 Aguilar, J., Cameron, T.A., Zupan, J., and Zambryski, P. (2011). Membrane and core periplasmic
621 *Agrobacterium tumefaciens* virulence Type IV secretion system components localise to multiple
622 sites around the bacterial perimeter during lateral attachment to plant cells. *MBio* 2, e00218-00211.
623 <https://doi.org/10.1128/mBio.00218-11>.
- 624 Al Mamun, A.A.M., Kishida, K., and Christie, P.J. (2021). Protein Transfer through an F Plasmid-
625 Encoded Type IV Secretion System Suppresses the Mating-Induced SOS Response. *MBio* 12,
626 e0162921. <https://doi.org/10.1128/mBio.01629-21>.
- 627 Althorpe, N.J., Chilley, P.M., Thomas, A.T., Brammar, W.J., and Wilkins, B.M. (1999a). Transient
628 transcriptional activation of the Inc11 plasmid anti-restriction gene (*ardA*) and SOS inhibition gene
629 (*psiB*) early in conjugating recipient bacteria. *Mol Microbiol* 31, 133–142.
630 <https://doi.org/10.1046/j.1365-2958.1999.01153.x>.
- 631 Althorpe, N.J., Chilley, P.M., Thomas, A.T., Brammar, W.J., and Wilkins, B.M. (1999b). Transient
632 transcriptional activation of the Inc11 plasmid anti-restriction gene (*ardA*) and SOS inhibition gene
633 (*psiB*) early in conjugating recipient bacteria. *Mol. Microbiol.* 31, 133–142.
634 <https://doi.org/10.1046/j.1365-2958.1999.01153.x>.
- 635 Babić, A., Lindner, A.B., Vulić, M., Stewart, E.J., and Radman, M. (2008). Direct Visualisation of
636 Horizontal Gene Transfer. *Science* 319, 1533–1536. <https://doi.org/10.1126/science.1153498>.
- 637 Babic, A., Berkmen, M.B., Lee, C.A., and Grossman, A.D. (2011). Efficient Gene Transfer in
638 Bacterial Cell Chains. *MBio* 2, e00027-11. <https://doi.org/10.1128/mBio.00027-11>.
- 639 Bagdasarian, M., Bailone, A., Angulo, J.F., Scholz, P., Bagdasarian, M., and Devoret, R. (1992).
640 PsiB, an anti-SOS protein, is transiently expressed by the F sex factor during its transmission to an
641 *Escherichia coli* K-12 recipient. *Molecular Microbiology* 6, 885–893.
642 <https://doi.org/10.1111/j.1365-2958.1992.tb01539.x>.
- 643 Baharoglu, Z., and Mazel, D. (2014). SOS, the formidable strategy of bacteria against aggressions.
644 *FEMS Microbiol. Rev.* 38, 1126–1145. <https://doi.org/10.1111/1574-6976.12077>.
- 645 Baharoglu, Z., Bikard, D., and Mazel, D. (2010). Conjugative DNA Transfer Induces the Bacterial
646 SOS Response and Promotes Antibiotic Resistance Development through Integron Activation.
647 *PLoS Genet* 6. <https://doi.org/10.1371/journal.pgen.1001165>.
- 648 Bailone, A., Bäckman, A., Sommer, S., Célérier, J., Bagdasarian, M.M., Bagdasarian, M., and
649 Devoret, R. (1988). PsiB polypeptide prevents activation of RecA protein in *Escherichia coli*. *Mol.*
650 *Gen. Genet.* 214, 389–395. <https://doi.org/10.1007/bf00330471>.
- 651 Barlow, M. (2009). What antimicrobial resistance has taught us about horizontal gene transfer.
652 *Methods Mol. Biol.* 532, 397–411. https://doi.org/10.1007/978-1-60327-853-9_23.
- 653 Bates, S., Roscoe, R.A., Althorpe, N.J., Brammar, W.J., and Wilkins, B.M. (1999). Expression of
654 leading region genes on Inc11 plasmid Collb-P9: genetic evidence for single-stranded DNA
655 transcription. *Microbiology* 145, 2655–2662. <https://doi.org/10.1099/00221287-145-10-2655>.

- 656 Benz, F., and Hall, A.R. (2022). Host-specific plasmid evolution explains the variable spread of
657 clinical antibiotic-resistance plasmids. *BioRxiv* 2022.07.06.498992.
658 <https://doi.org/10.1101/2022.07.06.498992>.
- 659 Beranek, A., Zettl, M., Lorenzoni, K., Schauer, A., Manhart, M., and Koraimann, G. (2004). Thirty-
660 eight C-terminal amino acids of the coupling protein TraD of the F-like conjugative resistance
661 plasmid R1 are required and sufficient to confer binding to the substrate selector protein TraM. *J.*
662 *Bacteriol.* *186*, 6999–7006. <https://doi.org/10.1128/JB.186.20.6999-7006.2004>.
- 663 Bouet, J.-Y., and Funnell, B.E. (2019). Plasmid Localisation and Partition in Enterobacteriaceae.
664 *EcoSal Plus* *8*. <https://doi.org/10.1128/ecosalplus.ESP-0003-2019>.
- 665 Carranza, G., Menguiano, T., Valenzuela-Gómez, F., García-Cazorla, Y., Cabezón, E., and
666 Arechaga, I. (2021). Monitoring Bacterial Conjugation by Optical Microscopy. *Front Microbiol* *12*,
667 750200. <https://doi.org/10.3389/fmicb.2021.750200>.
- 668 Cayron, J., and Lesterlin, C. (2019). Multi-scale Analysis of Bacterial Growth Under Stress
669 Treatments. *J Vis Exp* <https://doi.org/10.3791/60576>.
- 670 Chandler, M., de la Cruz, F., Dyda, F., Hickman, A.B., Moncalian, G., and Ton-Hoang, B. (2013).
671 Breaking and joining single-stranded DNA: the HUH endonuclease superfamily. *Nat. Rev.*
672 *Microbiol.* *11*, 525–538. <https://doi.org/10.1038/nrmicro3067>.
- 673 Christie, P.J., Whitaker, N., and González-Rivera, C. (2014). Mechanism and structure of the
674 bacterial type IV secretion systems. *Biochim Biophys Acta* *1843*, 1578–1591.
675 <https://doi.org/10.1016/j.bbamcr.2013.12.019>.
- 676 Clarke, M., Maddera, L., Harris, R.L., and Silverman, P.M. (2008). F-pili dynamics by live-cell
677 imaging. *Proc. Natl. Acad. Sci. U.S.A.* *105*, 17978–17981.
678 <https://doi.org/10.1073/pnas.0806786105>.
- 679 Clewell, D.B., and Helinski, D.E. (1970). Existence of the colicinogenic factor-sex factor ColI-b-P9
680 as a supercoiled circular DNA-protein relaxation complex. *Biochem. Biophys. Res. Commun.* *41*,
681 150–156. [https://doi.org/10.1016/0006-291x\(70\)90481-x](https://doi.org/10.1016/0006-291x(70)90481-x).
- 682 Cox, K.E.L., and Schildbach, J.F. (2017). Sequence of the R1 plasmid and comparison to F and
683 R100. *Plasmid* *91*, 53–60. <https://doi.org/10.1016/j.plasmid.2017.03.007>.
- 684 Cram, D., Ray, A., O’Gorman, L., and Skurray, R. (1984). Transcriptional analysis of the leading
685 region in F plasmid DNA transfer. *Plasmid* *11*, 221–233. [https://doi.org/10.1016/0147-](https://doi.org/10.1016/0147-619x(84)90028-3)
686 [619x\(84\)90028-3](https://doi.org/10.1016/0147-619x(84)90028-3).
- 687 Cruz, F.D.L., Frost, L.S., Meyer, R.J., and Zechner, E.L. (2010). Conjugative DNA metabolism in
688 Gram-negative bacteria. *FEMS Microbiology Reviews* *34*, 18–40. [https://doi.org/10.1111/j.1574-](https://doi.org/10.1111/j.1574-6976.2009.00195.x)
689 [6976.2009.00195.x](https://doi.org/10.1111/j.1574-6976.2009.00195.x).
- 690 Datsenko, K.A., and Wanner, B.L. (2000). One-step inactivation of chromosomal genes in
691 *Escherichia coli* K-12 using PCR products. *Proc. Natl. Acad. Sci. U.S.A.* *97*, 6640–6645.
692 <https://doi.org/10.1073/pnas.120163297>.
- 693 Di Lorenzo, L., Frost, L.S., and Paranchych, W. (1992). The TraM protein of the conjugative
694 plasmid F binds to the origin of transfer of the F and ColE1 plasmids. *Mol. Microbiol.* *6*, 2951–
695 2959. <https://doi.org/10.1111/j.1365-2958.1992.tb01754.x>.

- 696 Dostál, L., and Schildbach, J.F. (2010). Single-Stranded DNA Binding by F TraI Relaxase and
697 Helicase Domains Is Coordinately Regulated. *J Bacteriol* *192*, 3620–3628.
698 <https://doi.org/10.1128/JB.00154-10>.
- 699 Dostál, L., Shao, S., and Schildbach, J.F. (2011). Tracking F plasmid TraI relaxase processing
700 reactions provides insight into F plasmid transfer. *Nucleic Acids Res.* *39*, 2658–2670.
701 <https://doi.org/10.1093/nar/gkq1137>.
- 702 Draper, O., César, C.E., Machón, C., de la Cruz, F., and Llosa, M. (2005). Site-specific
703 recombinase and integrase activities of a conjugative relaxase in recipient cells. *Proc Natl Acad Sci*
704 *U S A* *102*, 16385–16390. <https://doi.org/10.1073/pnas.0506081102>.
- 705 Ducret, A., Quardokus, E.M., and Brun, Y.V. (2016). MicrobeJ, a tool for high throughput bacterial
706 cell detection and quantitative analysis. *Nat Microbiol* *1*, 16077.
707 <https://doi.org/10.1038/nmicrobiol.2016.77>.
- 708 Dutreix, M., Bäckman, A., Célérier, J., Bagdasarian, M.M., Sommer, S., Bailone, A., Devoret, R.,
709 and Bagdasarian, M. (1988). Identification of psiB genes of plasmids F and R6-5. Molecular basis
710 for psiB enhanced expression in plasmid R6-5. *Nucleic Acids Res.* *16*, 10669–10679.
711 <https://doi.org/10.1093/nar/16.22.10669>.
- 712 Everett, R., and Willetts, N. (1980). Characterisation of an in vivo system for nicking at the origin
713 of conjugal DNA transfer of the sex factor F. *J. Mol. Biol.* *136*, 129–150.
714 [https://doi.org/10.1016/0022-2836\(80\)90309-5](https://doi.org/10.1016/0022-2836(80)90309-5).
- 715 Fernandez-Lopez, R., de Toro, M., Moncalian, G., Garcillan-Barcia, M.P., and de la Cruz, F.
716 (2016). Comparative Genomics of the Conjugation Region of F-like Plasmids: Five Shades of F.
717 *Front. Mol. Biosci.* *3*. <https://doi.org/10.3389/fmolb.2016.00071>.
- 718 Fronzes, R., Christie, P.J., and Waksman, G. (2009). The structural biology of type IV secretion
719 systems. *Nat Rev Microbiol* *7*, 703–714. <https://doi.org/10.1038/nrmicro2218>.
- 720 Garcillán-Barcia, M.P., Jurado, P., González-Pérez, B., Moncalián, G., Fernández, L.A., and de la
721 Cruz, F. (2007). Conjugative transfer can be inhibited by blocking relaxase activity within recipient
722 cells with intrabodies. *Mol. Microbiol.* *63*, 404–416. [https://doi.org/10.1111/j.1365-
723 2958.2006.05523.x](https://doi.org/10.1111/j.1365-2958.2006.05523.x).
- 724 Garcillán-Barcia, M.P., Francia, M.V., and de La Cruz, F. (2009). The diversity of conjugative
725 relaxases and its application in plasmid classification. *FEMS Microbiol Rev* *33*, 657–687.
726 <https://doi.org/10.1111/j.1574-6976.2009.00168.x>.
- 727 Goldlust, K., Couturier, A., Terradot, L., and Lesterlin, C. (2022). Live-Cell Visualization of DNA
728 Transfer and Pilus Dynamics During Bacterial Conjugation. *Methods Mol Biol* *2476*, 63–74.
729 https://doi.org/10.1007/978-1-0716-2221-6_6.
- 730 Golub, E.I., and Low, K.B. (1985). Conjugative plasmids of enteric bacteria from many different
731 incompatibility groups have similar genes for single-stranded DNA-binding proteins. *J Bacteriol*
732 *162*, 235–241. .
- 733 Golub, E.I., and Low, K.B. (1986a). Unrelated conjugative plasmids have sequences which are
734 homologous to the leading region of the F factor. *J Bacteriol* *166*, 670–672.
735 <https://doi.org/10.1128/jb.166.2.670-672.1986>.

- 736 Golub, E.I., and Low, K.B. (1986b). Derepression of single-stranded DNA-binding protein genes
737 on plasmids derepressed for conjugation, and complementation of an *E. coli* *ssb*- mutation by these
738 genes. *Mol. Gen. Genet.* *204*, 410–416. <https://doi.org/10.1007/bf00331017>.
- 739 Golub, E., Bailone, A., and Devoret, R. (1988). A gene encoding an SOS inhibitor is present in
740 different conjugative plasmids. *J Bacteriol* *170*, 4392–4394. .
- 741 Gomis-Rüth, F.X., Solà, M., de la Cruz, F., and Coll, M. (2004). Coupling factors in
742 macromolecular type-IV secretion machineries. *Curr Pharm Des* *10*, 1551–1565.
743 <https://doi.org/10.2174/1381612043384817>.
- 744 Gordon, S., Rech, J., Lane, D., and Wright, A. (2004). Kinetics of plasmid segregation in
745 *Escherichia coli*. *Mol Microbiol* *51*, 461–469. <https://doi.org/10.1046/j.1365-2958.2003.03837.x>.
- 746 Grohmann, E., Muth, G., and Espinosa, M. (2003). Conjugative plasmid transfer in gram-positive
747 bacteria. *Microbiol. Mol. Biol. Rev.* *67*, 277–301, table of contents.
748 <https://doi.org/10.1128/membr.67.2.277-301.2003>.
- 749 Grohmann, E., Christie, P.J., Waksman, G., and Backert, S. (2018). Type IV secretion in Gram-
750 negative and Gram-positive bacteria. *Mol Microbiol* *107*, 455–471.
751 <https://doi.org/10.1111/mmi.13896>.
- 752 Howard, M.T., Nelson, W.C., and Matson, S.W. (1995). Stepwise assembly of a relaxosome at the
753 F plasmid origin of transfer. *J. Biol. Chem.* *270*, 28381–28386. .
- 754 Howland, C.J., Rees, C.E., Barth, P.T., and Wilkins, B.M. (1989). The *ssb* gene of plasmid Collb-
755 P9. *J. Bacteriol.* *171*, 2466–2473. <https://doi.org/10.1128/jb.171.5.2466-2473.1989>.
- 756 Hu, B., Khara, P., and Christie, P.J. (2019). Structural bases for F plasmid conjugation and F pilus
757 biogenesis in *Escherichia coli*. *Proc Natl Acad Sci U S A* *116*, 14222–14227.
758 <https://doi.org/10.1073/pnas.1904428116>.
- 759 Ilangovan, A., Kay, C.W.M., Roier, S., El Mkami, H., Salvadori, E., Zechner, E.L., Zanetti, G., and
760 Waksman, G. (2017). Cryo-EM Structure of a Relaxase Reveals the Molecular Basis of DNA
761 Unwinding during Bacterial Conjugation. *Cell* *169*, 708-721.e12.
762 <https://doi.org/10.1016/j.cell.2017.04.010>.
- 763 Jacob, F., and Wollman, E.L. (1958). Genetic and physical determinations of chromosomal
764 segments in *Escherichia coli*. *Symp. Soc. Exp. Biol.* *12*, 75–92. .
- 765 Jalajakumari, M.B., Guidolin, A., Buhk, H.J., Manning, P.A., Ham, L.M., Hodgson, A.L., Cheah,
766 K.C., and Skurray, R.A. (1987). Surface exclusion genes *traS* and *traT* of the F sex factor of
767 *Escherichia coli* K-12. Determination of the nucleotide sequence and promoter and terminator
768 activities. *J. Mol. Biol.* *198*, 1–11. [https://doi.org/10.1016/0022-2836\(87\)90452-9](https://doi.org/10.1016/0022-2836(87)90452-9).
- 769 Johnson, T.J., Danzeisen, J.L., Youmans, B., Case, K., Llop, K., Munoz-Aguayo, J., Flores-
770 Figueroa, C., Aziz, M., Stoesser, N., Sokurenko, E., et al. (2016). Separate F-Type Plasmids Have
771 Shaped the Evolution of the H30 Subclone of *Escherichia coli* Sequence Type 131. *MSphere* *1*,
772 e00121-16. <https://doi.org/10.1128/mSphere.00121-16>.
- 773 Jones, A.L., Barth, P.T., and Wilkins, B.M. (1992). Zygotic induction of plasmid *ssb* and *psiB*
774 genes following conjugative transfer of Inc11 plasmid Collb-P9. *Mol. Microbiol.* *6*, 605–613. .

- 775 Keasling, J.D., Palsson, B.O., and Cooper, S. (1991). Cell-cycle-specific F plasmid replication:
776 regulation by cell size control of initiation. *J Bacteriol* *173*, 2673–2680. .
- 777 Keasling, J.D., Palsson, B.O., and Cooper, S. (1992). Replication of mini-F plasmids during the
778 bacterial division cycle. *Research in Microbiology* *143*, 541–548. [https://doi.org/10.1016/0923-](https://doi.org/10.1016/0923-2508(92)90111-Z)
779 [2508\(92\)90111-Z](https://doi.org/10.1016/0923-2508(92)90111-Z).
- 780 Klimke, W.A., and Frost, L.S. (1998). Genetic analysis of the role of the transfer gene, traN, of the
781 F and R100-1 plasmids in mating pair stabilisation during conjugation. *J Bacteriol* *180*, 4036–4043.
782 <https://doi.org/10.1128/JB.180.16.4036-4043.1998>.
- 783 Kline, B.C. (1985). A review of mini-F plasmid maintenance. *Plasmid* *14*, 1–16.
784 [https://doi.org/10.1016/0147-619X\(85\)90027-7](https://doi.org/10.1016/0147-619X(85)90027-7).
- 785 Kolodkin, A.L., Capage, M.A., Golub, E.I., and Low, K.B. (1983). F sex factor of *Escherichia coli*
786 K-12 codes for a single-stranded DNA binding protein. *Proc Natl Acad Sci U S A* *80*, 4422–4426.
787 <https://doi.org/10.1073/pnas.80.14.4422>.
- 788 Lang, S., and Zechner, E.L. (2012). General requirements for protein secretion by the F-like
789 conjugation system R1. *Plasmid* *67*, 128–138. <https://doi.org/10.1016/j.plasmid.2011.12.014>.
- 790 Lanka, E., and Wilkins, B.M. (1995). DNA processing reactions in bacterial conjugation. *Annu Rev*
791 *Biochem* *64*, 141–169. <https://doi.org/10.1146/annurev.bi.64.070195.001041>.
- 792 Lanza, V.F., Toro, M. de, Garcillán-Barcia, M.P., Mora, A., Blanco, J., Coque, T.M., and Cruz, F.
793 de la (2014). Plasmid Flux in *Escherichia coli* ST131 Sublineages, Analysed by Plasmid
794 Constellation Network (PLACNET), a New Method for Plasmid Reconstruction from Whole
795 Genome Sequences. *PLOS Genetics* *10*, e1004766. <https://doi.org/10.1371/journal.pgen.1004766>.
- 796 Lawley, T.D., Gordon, G.S., Wright, A., and Taylor, D.E. (2002). Bacterial conjugative transfer:
797 visualisation of successful mating pairs and plasmid establishment in live *Escherichia coli*. *Mol*
798 *Microbiol* *44*, 947–956. <https://doi.org/10.1046/j.1365-2958.2002.02938.x>.
- 799 Lederberg, J., and Tatum, E.L. (1946). Gene recombination in *Escherichia coli*. *Nature* *158*, 558. .
- 800 Lesterlin, C., and Duabrry, N. (2016). Investigating Bacterial Chromosome Architecture. In
801 *Chromosome Architecture*, M.C. Leake, ed. (New York, NY: Springer New York), pp. 61–72.
- 802 Llosa, M., Gomis-Rüth, F.X., Coll, M., and de la Cruz Fd, F. (2002). Bacterial conjugation: a two-
803 step mechanism for DNA transport. *Mol. Microbiol.* *45*, 1–8. [https://doi.org/10.1046/j.1365-](https://doi.org/10.1046/j.1365-2958.2002.03014.x)
804 [2958.2002.03014.x](https://doi.org/10.1046/j.1365-2958.2002.03014.x).
- 805 Llosa, M., Zunzunegui, S., and de la Cruz, F. (2003). Conjugative coupling proteins interact with
806 cognate and heterologous VirB10-like proteins while exhibiting specificity for cognate
807 relaxosomes. *Proc. Natl. Acad. Sci. U.S.A.* *100*, 10465–10470.
808 <https://doi.org/10.1073/pnas.1830264100>.
- 809 Loh, S., Cram, D., and Skurray, R. (1989). Nucleotide sequence of the leading region adjacent to
810 the origin of transfer on plasmid F and its conservation among conjugative plasmids. *Molec. Gen.*
811 *Genet.* *219*, 177–186. <https://doi.org/10.1007/BF00261174>.
- 812 Loh, S., Skurray, R., Célérier, J., Bagdasarian, M., Bailone, A., and Devoret, R. (1990). Nucleotide
813 sequence of the psiA (plasmid SOS inhibition) gene located on the leading region of plasmids F and
814 R6-5. *Nucleic Acids Res* *18*, 4597. .

- 815 Loh, S.M., Cram, D.S., and Skurray, R.A. (1988). Nucleotide sequence and transcriptional analysis
816 of a third function (Flm) involved in F-plasmid maintenance. *Gene* 66, 259–268.
817 [https://doi.org/10.1016/0378-1119\(88\)90362-9](https://doi.org/10.1016/0378-1119(88)90362-9).
- 818 Lohman, T.M., and Ferrari, M.E. (1994). Escherichia coli single-stranded DNA-binding protein:
819 multiple DNA-binding modes and cooperativities. *Annu Rev Biochem* 63, 527–570.
820 <https://doi.org/10.1146/annurev.bi.63.070194.002523>.
- 821 Low, W.W., Wong, J.L.C., Beltran, L.C., Seddon, C., David, S., Kwong, H.-S., Bizeau, T., Wang,
822 F., Peña, A., Costa, T.R.D., et al. (2022). Mating pair stabilisation mediates bacterial conjugation
823 species specificity. *Nat Microbiol* 7, 1016–1027. <https://doi.org/10.1038/s41564-022-01146-4>.
- 824 Macé, K., Vadakkepat, A.K., Redzej, A., Lukoyanova, N., Oomen, C., Braun, N., Ukleja, M., Lu,
825 F., Costa, T.R.D., Orlova, E.V., et al. (2022). Cryo-EM structure of a type IV secretion system.
826 *Nature* 607, 191–196. <https://doi.org/10.1038/s41586-022-04859-y>.
- 827 Manning, P.A., Beutin, L., and Achtman, M. (1980). Outer membrane of Escherichia coli:
828 properties of the F sex factor traT protein which is involved in surface exclusion. *J. Bacteriol.* 142,
829 285–294. <https://doi.org/10.1128/JB.142.1.285-294.1980>.
- 830 Masai, H., and Arai, K. (1997). Frp: A Novel Single-Stranded DNA Promoter for Transcription
831 and for Primer RNA Synthesis of DNA Replication. *Cell* 89, 897–907.
832 [https://doi.org/10.1016/S0092-8674\(00\)80275-5](https://doi.org/10.1016/S0092-8674(00)80275-5).
- 833 Matson, S.W., and Morton, B.S. (1991). Escherichia coli DNA helicase I catalyses a site- and
834 strand-specific nicking reaction at the F plasmid oriT. *J. Biol. Chem.* 266, 16232–16237. .
- 835 Matson, S.W., and Ragonese, H. (2005). The F-plasmid TraI protein contains three functional
836 domains required for conjugative DNA strand transfer. *J. Bacteriol.* 187, 697–706.
837 <https://doi.org/10.1128/JB.187.2.697-706.2005>.
- 838 Moolman, M.C., Krishnan, S.T., Kerssemakers, J.W.J., van den Berg, A., Tulinski, P., Depken, M.,
839 Reyes-Lamothe, R., Sherratt, D.J., and Dekker, N.H. (2014). Slow unloading leads to DNA-bound
840 β 2-sliding clamp accumulation in live Escherichia coli cells. *Nat Commun* 5, 5820.
841 <https://doi.org/10.1038/ncomms6820>.
- 842 Nasim, M.T., Eperon, I.C., Wilkins, B.M., and Brammar, W.J. (2004). The activity of a single-
843 stranded promoter of plasmid ColIb-P9 depends on its secondary structure. *Mol Microbiol* 53, 405–
844 417. <https://doi.org/10.1111/j.1365-2958.2004.04114.x>.
- 845 Nelson, W.C., Morton, B.S., Lahue, E.E., and Matson, S.W. (1993). Characterisation of the
846 Escherichia coli F factor traY gene product and its binding sites. *J. Bacteriol.* 175, 2221–2228.
847 <https://doi.org/10.1128/jb.175.8.2221-2228.1993>.
- 848 Niki, H., and Hiraga, S. (1997). Subcellular distribution of actively partitioning F plasmid during
849 the cell division cycle in E. coli. *Cell* 90, 951–957. [https://doi.org/10.1016/s0092-8674\(00\)80359-1](https://doi.org/10.1016/s0092-8674(00)80359-1).
- 850 Nolivos, S., Cayron, J., Dedieu, A., Page, A., Delolme, F., and Lesterlin, C. (2019). Role of AcrAB-
851 TolC multidrug efflux pump in drug-resistance acquisition by plasmid transfer. *Science* 364, 778–
852 782. <https://doi.org/10.1126/science.aav6390>.
- 853 Penfold, S.S., Simon, J., and Frost, L.S. (1996). Regulation of the expression of the traM gene of
854 the F sex factor of Escherichia coli. *Mol. Microbiol.* 20, 549–558. <https://doi.org/10.1046/j.1365-2958.1996.5361059.x>.

- 856 Porter, R.D., and Black, S. (1991). The single-stranded-DNA-binding protein encoded by the
857 Escherichia coli F factor can complement a deletion of the chromosomal ssb gene. *J. Bacteriol.* *173*,
858 2720–2723. <https://doi.org/10.1128/jb.173.8.2720-2723.1991>.
- 859 Reyes-Lamothe, R., Possoz, C., Danilova, O., and Sherratt, D.J. (2008). Independent Positioning
860 and Action of Escherichia coli Replisomes in Live Cells. *Cell* *133*, 90–102.
861 <https://doi.org/10.1016/j.cell.2008.01.044>.
- 862 Reyes-Lamothe, R., Sherratt, D.J., and Leake, M.C. (2010). Stoichiometry and architecture of
863 active DNA replication machinery in Escherichia coli. *Science* *328*, 498–501.
864 <https://doi.org/10.1126/science.1185757>.
- 865 Reygers, U., Wessel, R., Müller, H., and Hoffmann-Berling, H. (1991). Endonuclease activity of
866 Escherichia coli DNA helicase I directed against the transfer origin of the F factor. *EMBO J.* *10*,
867 2689–2694. .
- 868 Schildbach, J.F., Robinson, C.R., and Sauer, R.T. (1998). Biophysical characterisation of the TraY
869 protein of Escherichia coli F factor. *J. Biol. Chem.* *273*, 1329–1333.
870 <https://doi.org/10.1074/jbc.273.3.1329>.
- 871 Schröder, G., and Lanka, E. (2005). The mating pair formation system of conjugative plasmids-A
872 versatile secretion machinery for transfer of proteins and DNA. *Plasmid* *54*, 1–25.
873 <https://doi.org/10.1016/j.plasmid.2005.02.001>.
- 874 Sikora, B., Eoff, R.L., Matson, S.W., and Raney, K.D. (2006). DNA unwinding by Escherichia coli
875 DNA helicase I (TraI) provides evidence for a processive monomeric molecular motor. *J. Biol.*
876 *Chem.* *281*, 36110–36116. <https://doi.org/10.1074/jbc.M604412200>.
- 877 Stephens, K.M., and McMacken, R. (1997). Functional properties of replication fork assemblies
878 established by the bacteriophage lambda O and P replication proteins. *J Biol Chem* *272*, 28800–
879 28813. <https://doi.org/10.1074/jbc.272.45.28800>.
- 880 Tatum, E.L., and Lederberg, J. (1947). Gene Recombination in the Bacterium Escherichia coli. *J.*
881 *Bacteriol.* *53*, 673–684. .
- 882 Thomas, C.M. (2000). Paradigms of plasmid organisation. *Mol Microbiol* *37*, 485–491.
883 <https://doi.org/10.1046/j.1365-2958.2000.02006.x>.
- 884 Traxler, B.A., and Minkley, E.G. (1988). Evidence that DNA helicase I and oriT site-specific
885 nicking are both functions of the F TraI protein. *J. Mol. Biol.* *204*, 205–209.
886 [https://doi.org/10.1016/0022-2836\(88\)90609-2](https://doi.org/10.1016/0022-2836(88)90609-2).
- 887 Verhoeven, G.S., Dogterom, M., and den Blaauwen, T. (2013). Absence of long-range diffusion of
888 OmpA in E. coliis not caused by its peptidoglycan binding domain. *BMC Microbiology* *13*, 66.
889 <https://doi.org/10.1186/1471-2180-13-66>.
- 890 Virolle, C., Goldlust, K., Djermoun, S., Bigot, S., and Lesterlin, C. (2020). Plasmid Transfer by
891 Conjugation in Gram-Negative Bacteria: From the Cellular to the Community Level. *Genes (Basel)*
892 *11*. <https://doi.org/10.3390/genes11111239>.
- 893 Wawrzyniak, P., Plucienniczak, G., and Bartosik, D. (2017). The Different Faces of Rolling-Circle
894 Replication and Its Multifunctional Initiator Proteins. *Front Microbiol* *8*, 2353.
895 <https://doi.org/10.3389/fmicb.2017.02353>.

- 896 Westra, E.R., Staals, R.H.J., Gort, G., Høgh, S., Neumann, S., de la Cruz, F., Fineran, P.C., and
897 Brouns, S.J.J. (2013). CRISPR-Cas systems preferentially target the leading regions of MOBF
898 conjugative plasmids. *RNA Biology* *10*, 749–761. <https://doi.org/10.4161/rna.24202>.
- 899 Willetts, N., and Skurray, R. (1980). The conjugation system of F-like plasmids. *Annu. Rev. Genet.*
900 *14*, 41–76. <https://doi.org/10.1146/annurev.ge.14.120180.000353>.
- 901 Yu, D., Ellis, H.M., Lee, E.C., Jenkins, N.A., Copeland, N.G., and Court, D.L. (2000). An efficient
902 recombination system for chromosome engineering in *Escherichia coli*. *Proc. Natl. Acad. Sci.*
903 *U.S.A.* *97*, 5978–5983. <https://doi.org/10.1073/pnas.100127597>.
- 904

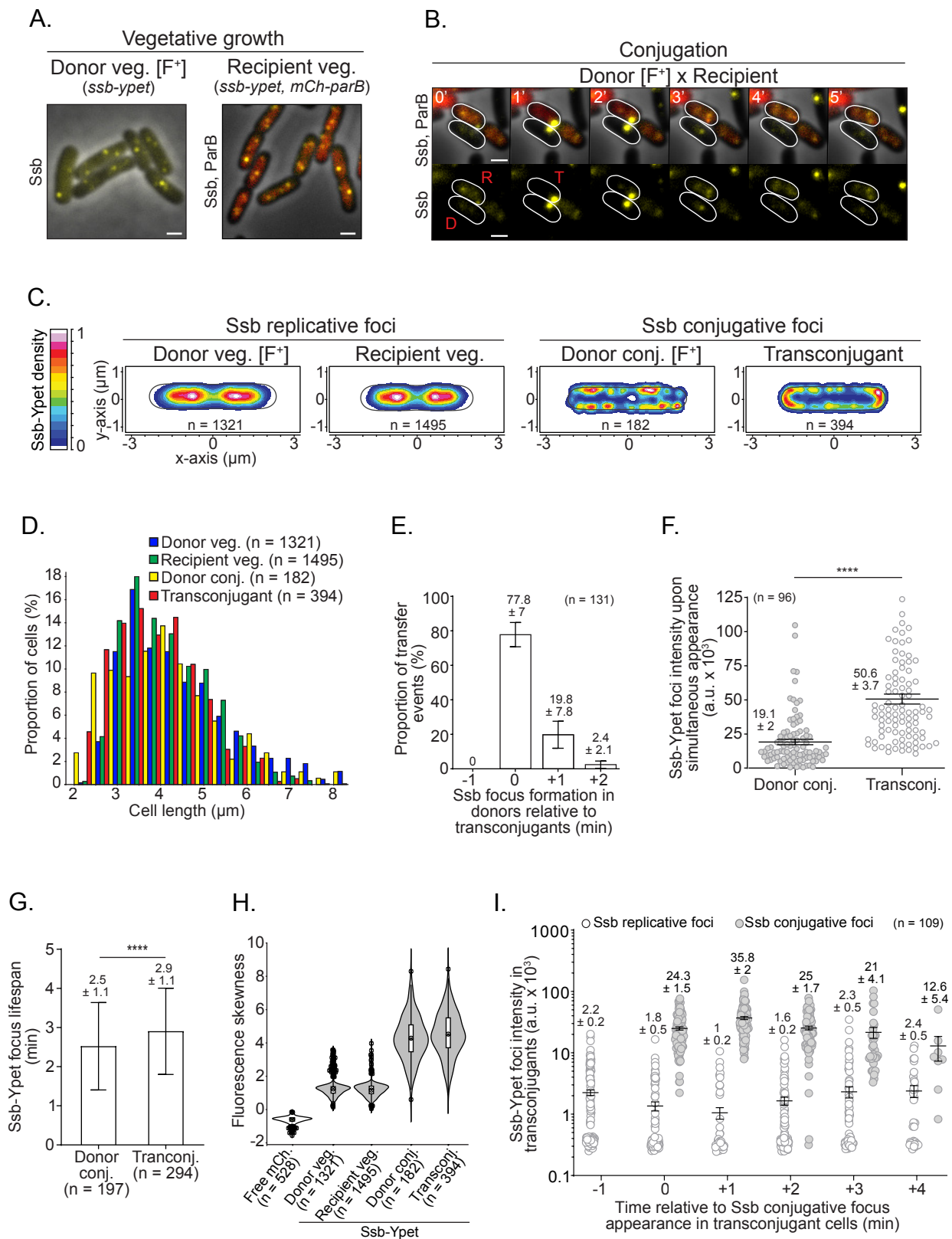


Figure 1

Figure 1. Real time dynamics of ssDNA plasmid transfer from donor to recipient cells.

(A) Snapshot microscopy imaging of donor and recipient strains carrying the endogenous *ssb-yjet* fusion gene on the chromosome during vegetative growth. The recipient cells also produce the mCh-ParB fluorescent protein from the pSN70 plasmid that diffuses freely into the cytoplasm in the absence of the F plasmid carrying the *parS*-binding site. Scale bars 1 μ m. (B) Time-lapse microscopy images of conjugation performed in microfluidic chamber showing a plasmid transfer event between a donor (D) and a recipient cell (R) that is converted into a transconjugant (T). The ssDNA plasmid transfer is reported by the formation of paired bright membrane-associated Ssb-Yjet foci in both donor and transconjugant cells. Scale bars 1 μ m. Additional transfer events are presented in Figure S1. (C) 2D localisation heatmaps of Ssb-Yjet fluorescent protein in donor, recipient cells in vegetative growth and in donor and transconjugant cells during conjugation. Heatmaps correspond to the merge and normalisation by the cell length of (n) individual cells from at least three biological replicates. The density scale bar is shown on the left. (D) Cell length distribution histogram of donor and recipient cells during vegetative growth, and of donor and transconjugant cells during conjugation (n cells analysed from at least three independent experiments). (E) Apparition timing of the Ssb conjugative focus in donor relative to transconjugant cells. Histograms represent the proportion of individual transfer events in which the Ssb focus appears in the donors before (-1 min), at the same time of (0 min) or after (+1 min; +2 min) the formation of a Ssb focus in the transconjugants. The number (n) of individual transfer events analysed from three independent experiments is indicated. (F) Jitter plot of the fluorescence intensity of Ssb-Yjet conjugative foci upon simultaneous formation in donor and transconjugant cells. The number of foci analysed from three independent experiments (n) is indicated. *P*-value significance from Mann-Whitney statistical test is indicated by ****($P \leq 0.0001$). (G) Histograms of Ssb-Yjet conjugative foci lifespan in donor and transconjugant cells measured at the single-cell level. *P*-value significance from Mann-Whitney statistical test is indicated by ****($P = 0.0001$). The number (n) of cells analysed from at least five independent experiments is indicated. (H) Violin plots showing the fluorescence skewness of a free mCherry produced from a plasmid and of the chromosomally encoded Ssb-Yjet in donor and recipient cells during vegetative growth or donor and transconjugant cells during conjugation. The median, quartile 1 and quartile 3 are indicated by horizontal lines and the mean by a black dot. Black dots above and below the max and min values correspond to outlier cells. The number of cells analysed (n) from one representative experiment is indicated. (I) Jitter plot showing the evolution of the intensity of Ssb-Yjet replicative and conjugative foci in transconjugant cells in the course of the conjugation process. Time 0 minute corresponds to the appearance of the Ssb-Yjet conjugative focus in recipient cells. The number of cells analysed (n) from three independent experiments is indicated. Donor (LY1007), recipient (LY358), transconjugant (LY358 after *Fwt* acquisition from LY1007); free mCherry producing strain (LY318).

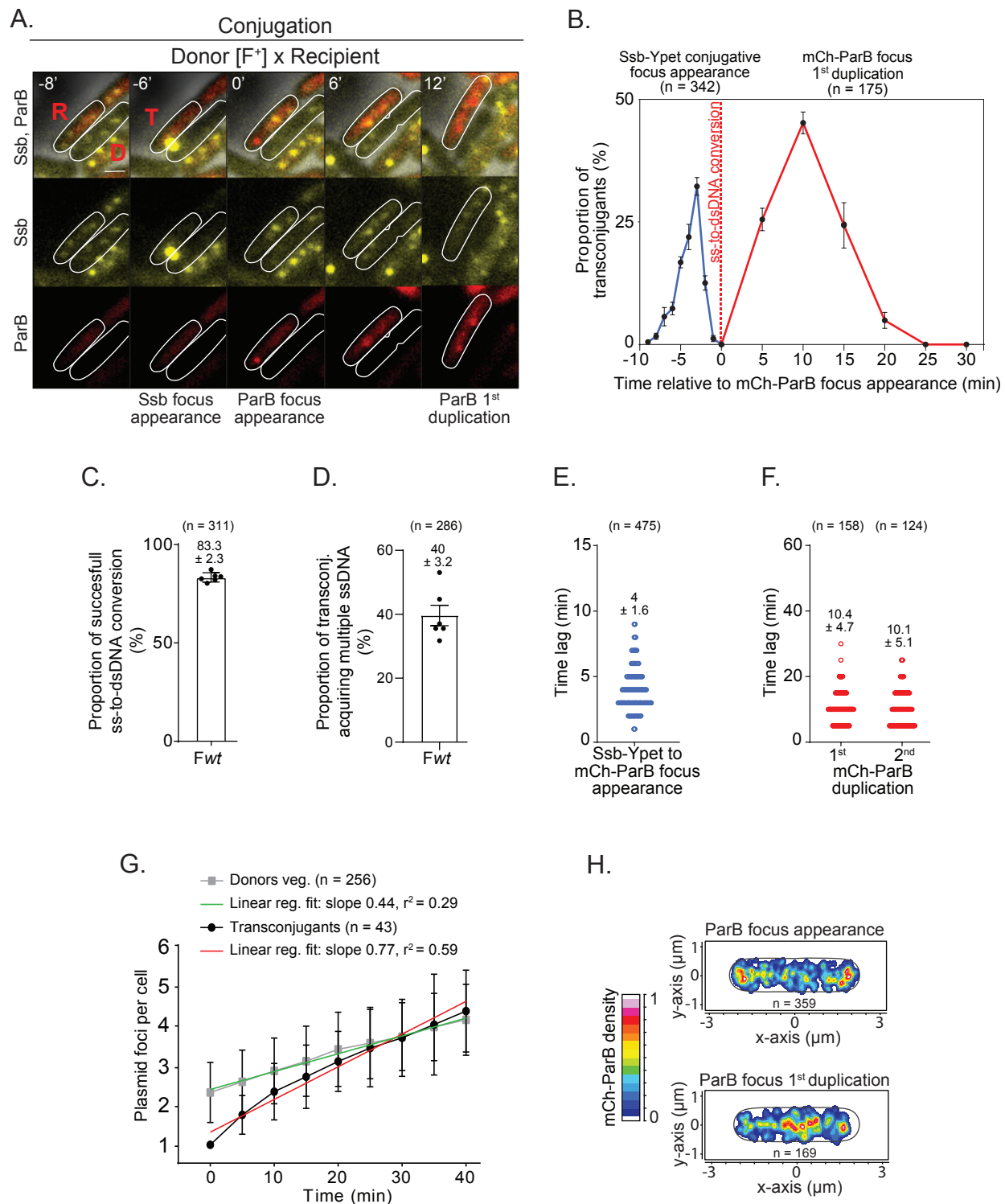


Figure 2

Figure 2. Timing and spatial localisation of the ss-to-dsDNA conversion and plasmid duplication in transconjugant cells.

(A) Time-lapse microscopy images performed in microfluidic chamber showing the transfer of the ssDNA plasmid reported by the formation of the Ssb-Ypet conjugative foci in both donor (D) and recipient (R) cells, followed by the ss-to-dsDNA conversion reflected by the appearance of a mCh-ParB focus in transconjugant (T) cells. Scale bar 1 μm . (B) Single-cell time-lapse quantification of Ssb-Ypet focus appearance (blue line) and mCh-ParB focus first duplication (red line) with respect to the ss-to-dsDNA conversion revealed by mCh-ParB focus formation in transconjugant cells (0 min). The number of conjugation events analysed (n) from seven independent experiments is indicated. (C) Histogram showing the frequency of successful ss-to-dsDNA conversion reflected by the conversion of the Ssb-Ypet conjugative foci into a mCh-ParB focus. The mean and SD are calculated from (n) individual transfer events from six biological replicates (black dots). (D) Histogram showing the percentage of transconjugant cells with a mCh-ParB focus that acquire multiple ssDNA plasmids as revealed by the successive appearance of an additional Ssb-Ypet conjugative focus. The mean and SD are calculated from (n) individual transconjugant cells from six biological replicates (black dots). (E) Scatter plot showing the time lag between the appearance of the Ssb-Ypet focus and the mCh-ParB focus in transconjugant cells. The mean and SD calculated from (n) individual ss-to-dsDNA conversion event (blue circles) from seven biological replicates are indicated. (F) Scatter plot showing the time-lag between the apparition of the mCh-ParB focus and its visual duplication in two foci (1st duplication), and in three or four foci (2nd duplication). The mean and SD calculated from (n) individual duplication events (red circles) from at least six biological replicates are indicated. (G) Single-cell time-lapse quantification of the number of F foci per cell in F-carrying donor strain during vegetative growth and in transconjugants after F plasmid acquisition. For donor, the number of F foci per cell (reflected by the number of SopB-sfGFP foci) with respect to cells birth ($t = 0$ min) is shown (grey curve). For transconjugants the number of F foci per cell (reflected by the number of mCh-ParB foci) with respect to mCh-ParB focus appearance ($t = 0$ min) is shown (black curve). Mean and SD calculated from (n) individual cells from four biological replicates are indicated, together with curves' linear fitting lines for donors (green) and transconjugants (red). F-carrying donor strain (LY834), Transconjugant (LY358 after Fwt acquisition). (H) 2D localisation heatmaps of the mCh-ParB focus at the time of its appearance (top) and just before its duplication into two foci (bottom). Heatmaps correspond to the merge and normalisation by the cell length of (n) individual transconjugant cells from seven biological replicates. (A-F and H) Fwt donor (LY1007), recipient (LY358), transconjugant (LY358 after Fwt acquisition).

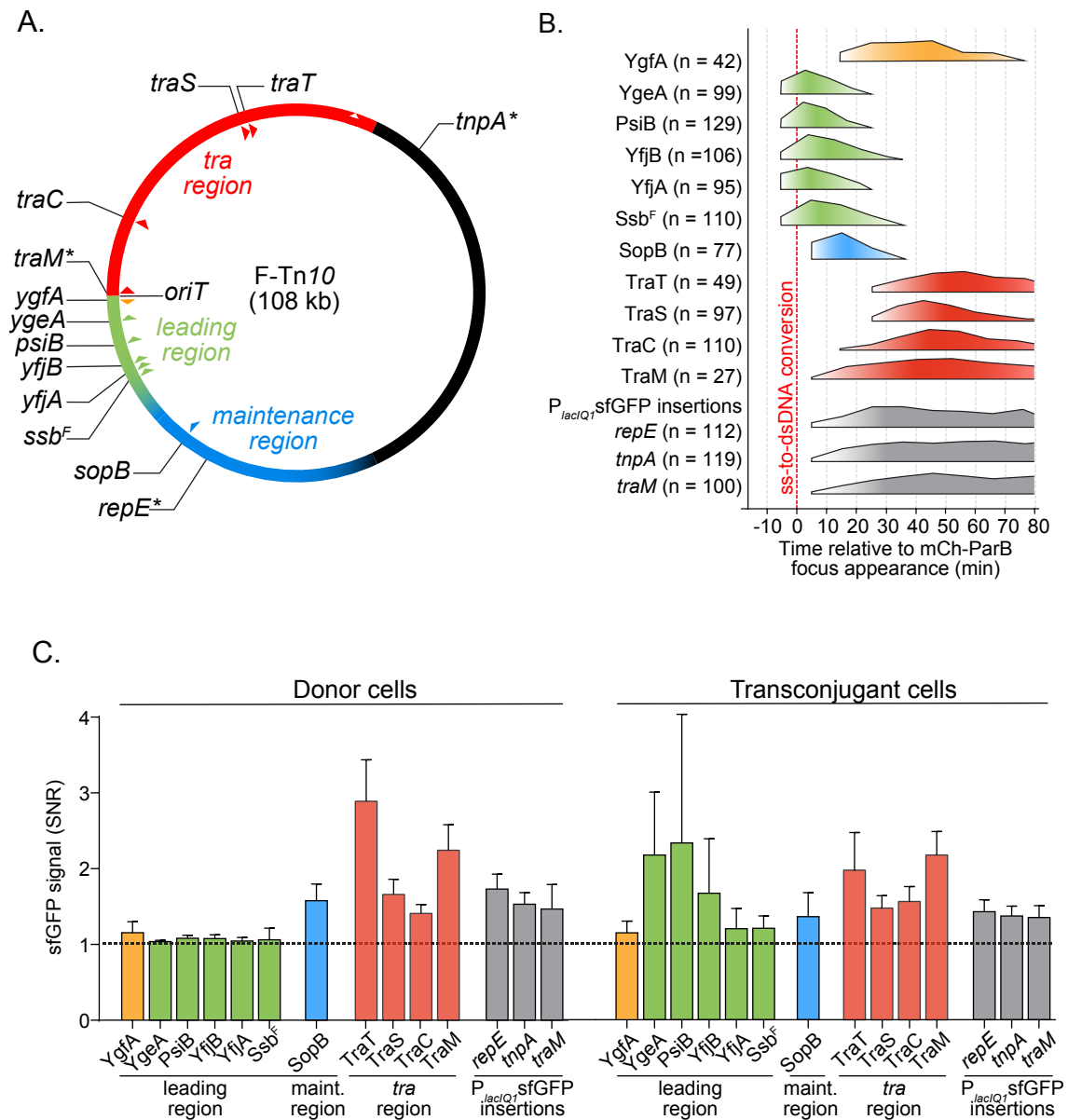


Figure 3

Figure 3. Timing of plasmid-encoded proteins production in transconjugant cells.

(A) Genetic map of the 108 kb F plasmid indicating the leading (green), Tra (red) and maintenance (blue) regions, and the positions of the studied genes (triangles). Stars represent the genetic location of the $P_{lacIQ1}sfGFP$ insertions. (B) Summary diagram of the production timing of each plasmid-encoded protein fusions in transconjugant cells with respect to the timing of ss-to-dsDNA conversion reflected by mCh-ParB focus appearance (0 min). The diagram represent data from the foldchange increase in sfGFP signal from Figure S5. Orange/green, blue and red colours correspond to production of proteins from the leading, maintenance and transfer region respectively. Timings of the cytoplasmic sfGFP production from the P_{lacIQ1} promoter inserted in the *repE-sopA* (*repE*), *tnpA-ybaA* (*tnpA*) and *traM-traJ* (*traM*) intergenic regions are represented in grey. The number (n) of individual transconjugant cells from at least three biological replicates analysed is indicated. (C) Histograms showing the intracellular green fluorescence (SNR) for each sfGFP fusions and reporters within vegetatively growing donor (left) and transconjugant cells (right) at the maximum SNR value from Figure S5. Means and SD calculated from the same individual transconjugant cells as in (B) are indicated. Donors of F derivatives (see Table S1), Recipient (LY358).

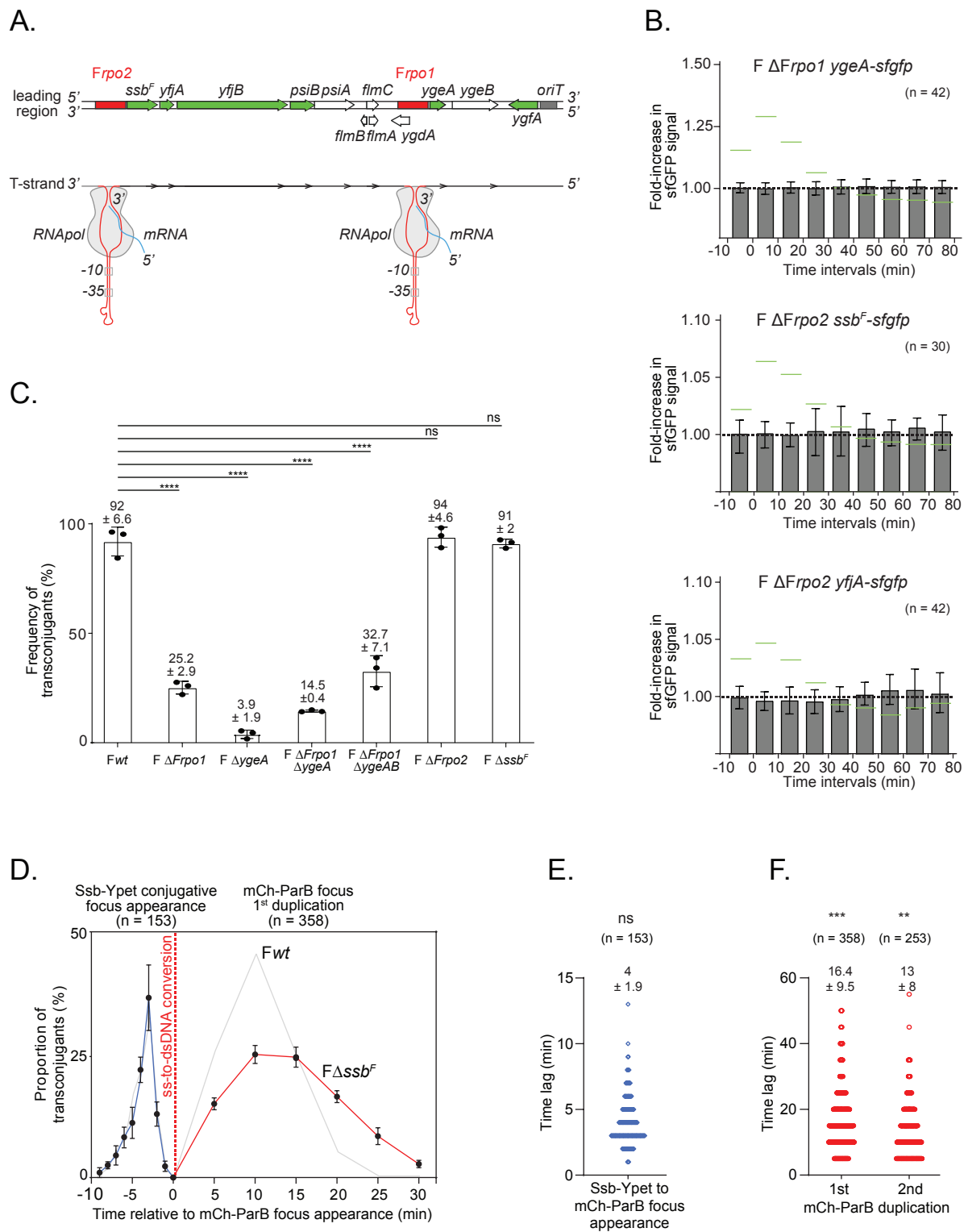
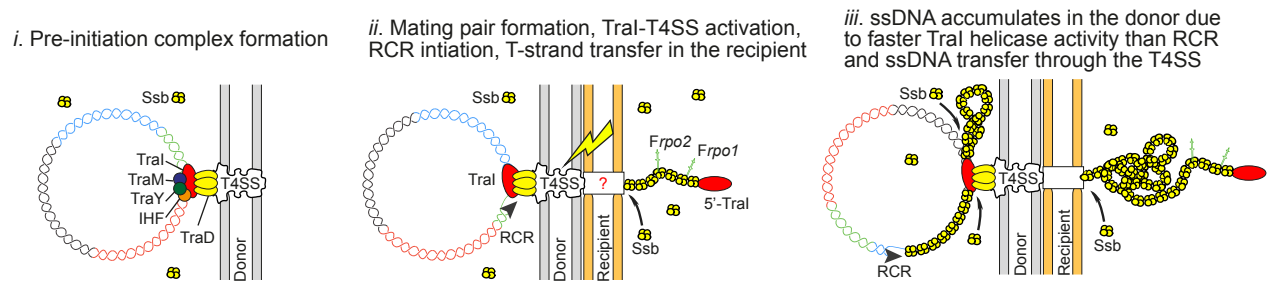


Figure 4

Figure 4. Role of leading region factors *Frpo1*, *Frpo2* and *ssb^F* in conjugation.

(A) Genetic map of the dsDNA leading region showing the position of the genes (green for studied sfGFP fusions and white for the other genes) and *Frpo1* and *Frpo2* promoters (red) (top). The bottom diagram shows the stem-loop structure formed by the ssDNA forms of *Frpo1* and *Frpo2* promoter sequences (detailed in Figure S6). Recognition of the -10 and -35 boxes present in the dsDNA stem region by the RNA polymerase (RNA pol in grey) induces the initiation of transcription and the production of mRNA (blue). (B) Histograms of intracellular sfGFP fold increase in transconjugant after acquisition of F $\Delta Frpo1$ *ygeA-sfgfp*, F $\Delta Frpo2$ *ssb-sfgfp* and F $\Delta Frpo2$ *yjJA-sfgfp*. Mean and SD are calculated from (n) individual transconjugant cells analysed from at least three independent experiments. Levels obtained with the *Fwt* plasmid from Figure S5A are *wt* reported in green as a reference. Donor of F $\Delta Frpo1$ *ygeA-sfgfp* (LY1368), F $\Delta Frpo2$ *ssb-sfgfp* (LY1365), F $\Delta Frpo2$ *yjJA-sfgfp* (LY1364), recipient (LY318). (C) Histograms of *Fwt*, deletion mutants F $\Delta Frpo1$, F $\Delta ygeA$, F $\Delta Frpo1$ $\Delta ygeA$, F $\Delta Frpo1$ $\Delta ygeAB$, F $\Delta Frpo2$ and F Δssb^F frequency of transconjugant (T/R+T) estimated by plating assays. Mean and SD are calculated from at least three independent experiments. *P*-value significance ns and *****P* \leq 0.0001 were obtained from One-way ANOVA with Dunnetts multiple comparisons test. Donor of *Fwt* (LY875), F $\Delta Frpo1$ (LY824), F $\Delta ygeA$ (LY160), F $\Delta Frpo1$ $\Delta ygeA$ (LY1424), F $\Delta Frpo1$ $\Delta ygeAB$ (LY1425), F $\Delta Frpo2$ (LY823), F Δssb^F (LY755), recipient (MS428). (D) Single-cell time-lapse quantification of *Ssb*-Ypet focus appearance (blue line) and mCh-ParB focus first duplication (red line) with respect to the ss-to-dsDNA conversion revealed by mCh-ParB focus formation in transconjugant cells (0 min) that receive the F Δssb^F plasmid. The number of conjugation events analysed (n) from five independent biological replicates is indicated. Results obtained in Figure 2B with *Fwt* plasmid are reported in grey for comparison. (E) Scatter plot showing the time lag between the appearance of the *Ssb*-Ypet focus and the appearance of the mCh-ParB focus in transconjugant cells after the acquisition of the F Δssb^F plasmid. The mean and SD calculated from (n) individual ss-to-dsDNA conversion event (blue circles) from five biological replicates are indicated. *P*-value significance ns (>0.05 non-significant) was obtained from Mann-Whitney statistical test against results obtained with the *Fwt* plasmid (Figure 2E). (F) Scatter plot showing the time-lag between the apparition of the mCh-ParB focus and its visual duplication in two foci (1st duplication), and in three or four foci (2nd duplication) in transconjugant cells after acquisition of the F Δssb^F plasmid. The mean and SD calculated from (n) individual duplication events (red circles) from eight biological replicates are indicated. *P*-value significance ***P* = 0.0023 and ****P* = 0.0007 were obtained from Mann-Whitney statistical test against results obtained with the *Fwt* plasmid (Figure 2F). Donor F Δssb^F (LY1068), recipient (LY358).

A.



B.

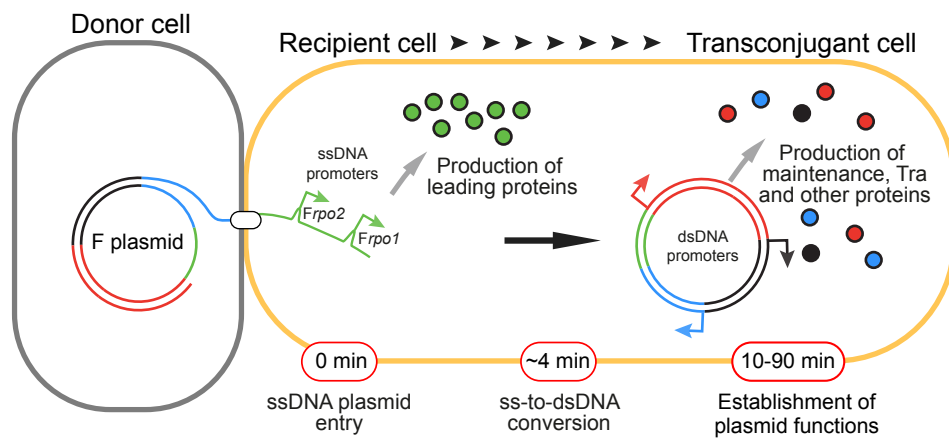


Figure 5

Figure 5. Model for conjugation initiation and intracellular dynamics.

(A) (i) Before the initiation of conjugation, the pre-initiation complex bound to the plasmid's origin of transfer is docked to the Type IV secretion system (T4SS). (ii) The establishment of the mating pair transduces a signal that activates the pre-initiation complex. Unwinding of the dsDNA plasmid by the helicase activity of TraI produces the first segment of the T-strand, which is immediately transferred into the recipient cell where it recruits Ssb molecules, while the non-transferred strand is being complemented by rolling-circle replication (RCR) in the donor cell. (iii) The helicase activity of TraI generates ssDNA at higher rate than the T-strand is transferred through the T4SS or the non-transferred strand is complemented by RCR, thus resulting in the accumulation of ssDNA plasmid coated by Ssb molecules in the donor cell. **(B)** Upon entry of the ssDNA plasmid in the recipient cell, *Frpo1* and *Frpo2* leading sequences form stem-loop structures that serve as promoters initiating the transcription of the downstream leading genes, rapidly resulting in the production of leading proteins. The subsequent ss-to-dsDNA conversion inactivates *Frpo1* and *Frpo2* and licenses the expression of other plasmid genes under the control of conventional dsDNA promoters. The production of maintenance, transfer and other plasmid-encoded proteins eventually results in the development of new functions by the transconjugant cell.